

Experiment and numerical study of the charge decay on the surface of PMMA
insulator



A Thesis Submitted in Partial Fulfillment of the Requirements
for the Degree of Master of Engineering in Electrical Engineering

Department of Electrical Engineering

FACULTY OF ENGINEERING

Chulalongkorn University

Academic Year 2020

Copyright of Chulalongkorn University

การทดลองและการศึกษาเชิงตัวเลขของการสลายประจุบนผิวฉนวนพืเอ็มเอ็มเอ



วิทยานิพนธ์นี้เป็นส่วนหนึ่งของการศึกษาตามหลักสูตรปริญญาวิศวกรรมศาสตรมหาบัณฑิต
สาขาวิชาวิศวกรรมไฟฟ้า ภาควิชาวิศวกรรมไฟฟ้า
คณะวิศวกรรมศาสตร์ จุฬาลงกรณ์มหาวิทยาลัย
ปีการศึกษา 2563
ลิขสิทธิ์ของจุฬาลงกรณ์มหาวิทยาลัย

กมลพร มาลาทิพย์ : การทดลองและการศึกษาเชิงตัวเลขของการสลายประจุบนผิวฉนวนพีเอ็มเอ็มเอ.
(Experiment and numerical study of the charge decay on the surface of PMMA
insulator) อ.ที่ปรึกษาหลัก : ศ. ดร.บุญชัย เตชะอำนาจ

วิทยานิพนธ์นี้นำเสนอการวัดและการจำลองการลดลงของประจุไฟฟ้าบนแผ่นพอลิเมทิลเมทาคริเลต (PMMA). วัตถุประสงค์ของวิทยานิพนธ์คือ การคำนวณความหนาแน่นของประจุไฟฟ้าในแบบจำลอง 2 มิติและแบบจำลอง 3 มิติ เพื่อเปรียบเทียบกับผลประมาณที่ได้จากการทดลอง, และเพื่อศึกษากลไกของประจุซึ่งขึ้นอยู่กับ ความหนาของแผ่นไดอิเล็กทริก สำหรับการทดลอง การจัดเรียงอิเล็กโทรดแบบระนาบ-แบบแท่งถูกใช้เพื่อสร้างการปลดปล่อยโคโรนาชั่วคราวบนผิวของแผ่น PMMA ที่มีความหนา 1, 2 และ 10 มม. ค่าศักย์ไฟฟ้าพื้นผิวที่วัดได้ถูกนำมาใช้ในการคำนวณสนามไฟฟ้าโดยใช้วิธีไฟไนต์เอลิเมนต์ (FEM) ความหนาแน่นของประจุที่พื้นผิวคำนวณจากองค์ประกอบสนามไฟฟ้า การกระจายค่าศักย์ไฟฟ้าพื้นผิวเริ่มแรกเป็นรูประฆังแล้วสลายไปตามกาลเวลา ค่าศักย์ไฟฟ้าพื้นผิวในกรณีที่มีความหนา 10 มม. ลดลงเร็วกว่าในกรณีที่บางกว่า ปรากฏการณ์ทางกายภาพที่เกี่ยวข้องกับการลดประจุที่พื้นผิวคือ 1. การทำให้เป็นกลางของประจุ 2. การนำทางพื้นผิว และ 3. การนำทางปริมาตร ในทุกกรณีของความหนา, ความหนาแน่นของประจุที่พื้นผิวลดลงอย่างมากที่ตำแหน่งกลาง และจากนั้นเป็นรูปร่างคล้ายปล่องภูเขาไฟ. อันเนื่องมาจากกลไกการทำให้เป็นกลางของประจุ ในกรณีของความหนา 1 และ 2 มม. ความหนาแน่นของประจุจะกระจายไปในตำแหน่งแนวรัศมีของแผ่น PMMA ตามกลไกการนำเชิงพื้นผิว นอกจากนี้ การกระจายประจุที่พื้นผิวลดลงโดยรวมเนื่องจากกลไกของการนำเชิงปริมาตร

จุฬาลงกรณ์มหาวิทยาลัย
CHULALONGKORN UNIVERSITY

สาขาวิชา วิศวกรรมไฟฟ้า
ปีการศึกษา 2563

ลายมือชื่อนิสิต

ลายมือชื่อ อ.ที่ปรึกษาหลัก

6170104921 : MAJOR ELECTRICAL ENGINEERING

KEYWORD: Surface charge decay Polymethyl methacrylate Charge decay mechanism

Kamonporn Malathip : Experiment and numerical study of the charge decay on the surface of PMMA insulator. Advisor: Prof. Boonchai Techaumnat, Ph.D.

This thesis presents the measurement and simulation of surface charge decay on a polymethyl methacrylate (PMMA) circular disc. The objective of the thesis is to calculate the surface charge density in the 2-dimensional (2D) and the 3-dimensional (3D) models for comparison with the estimated results obtained from experiments, and to study the mechanisms of charge which depends on the thickness of the dielectric disc. For the experiments, a rod-plane electrode arrangement was used to generate the positive corona discharge on surface of 1-, 2- and 10-mm thick PMMA disc. The measured surface potential was used to calculate the electric field by using the finite element method (FEM). The surface charge density was calculated from the electric field component. The surface potential distribution was initially bell-shaped then decayed with time. The surface potential in the case of 10-mm thickness decreased faster than that in the thinner cases. The physical phenomena related to the surface charge reduction were 1. charge neutralization, 2. surface conduction, and 3. volume conduction. In all cases of thickness, the surface charge density was remarkably decreased at the center position and then made as a crater-like shape due to the charge neutralization mechanism. In the case of 1- and 2-mm thickness, the charge density spread in the radial position of PMMA disc according to the surface conduction mechanism. Furthermore, the surface charge distribution was sunk overall due to the mechanism of volume conduction.

จุฬาลงกรณ์มหาวิทยาลัย
CHULALONGKORN UNIVERSITY

Field of Study: Electrical Engineering

Student's Signature

Academic Year: 2020

Advisor's Signature

ACKNOWLEDGEMENTS

The author acknowledge the Fukuoka University Scholarship for International students

Kamonporn Malathip



TABLE OF CONTENTS

	Page
ABSTRACT (THAI).....	iii
ABSTRACT (ENGLISH).....	iv
ACKNOWLEDGEMENTS.....	v
TABLE OF CONTENTS.....	vi
LIST OF TABLES.....	viii
LIST OF FIGURES.....	ix
CHAPTER 1.....	1
INTRODUCTION.....	1
1.1 General introduction.....	1
1.2 Literature review.....	2
1.3 Objectives of the thesis.....	8
1.4 Scope of the thesis.....	8
1.5 Expected outcome.....	8
CHAPTER 2.....	9
THEORY.....	9
2.1 Discharge and accumulation of charges.....	9
2.2 Electric field simulation.....	9
2.3 Finite element method (FEM).....	12
CHAPTER 3.....	15
EXPERIMENT.....	15
3.1 Experimental method.....	15

3.2 Measurement procedure.....	17
CHAPTER 4.....	20
SIMULATION	20
4.1 2D simulation	20
4.2 3D simulation	24
CHAPTER 5.....	28
RESULTS AND DISCUSSION.....	28
5.1 Experiment results	28
5.2 Simulation results	32
5.2.2 3D simulation.....	34
5.2.2.1 1-mm thickness PMMA disc.....	35
5.2.2.2 2-mm thickness PMMA disc.....	37
CHAPTER 6.....	41
CONCLUSIONS.....	41
6.1 Measurement results	41
6.2 2D simulation results	41
6.3 3D simulation results	42
REFERENCES	43
Appendix A.....	45
Appendix B.....	49
VITA.....	50

LIST OF TABLES

	Page
Table 1 The total surface charge and different of charge on a 1, 2 and 10-mm thick PMMA disc.....	40



LIST OF FIGURES

	Page
Figure 1 Experiment setup (1-HVDC generator, 2-Bushing, 3-GIS transfer unit,.....	6
Figure 2 3-dimensional model of PMMA sheet placed on plane electrode.....	11
Figure 3 Triangular element.....	12
Figure 4 Rectangular element.....	13
Figure 5 Tetrahedral element.....	14
Figure 6 1-mm thick PMMA disc.....	15
Figure 7 Static eliminator (495, HAKKA).....	16
Figure 8 Schematic drawing of experiment setup [14].....	16
Figure 9 Rod-plane electrode configuration.....	17
Figure 10 Measurement system.....	18
Figure 11 Configuration of surface charge measurement.....	18
Figure 12 Measurement probe.....	19
Figure 13 2-dimensional axisymmetric models (dimensions are in mm.).....	20
Figure 14 Meshed 2-dimensional model through the GiD program.....	20
Figure 15 Division of the PMMA disc in 0.5-centimeter grids.....	21
Figure 16 Linear interpolation for the 2D model.....	22
Figure 17 Sif file calling interpolating function for Elmer.....	23
Figure 18 Setting for the 2-dimensional model in Elmer.....	23
Figure 19 Geometry of 3D model and toolbox menu of GiD.....	24
Figure 20 3D calculation model (dimensions are in mm.).....	25
Figure 21 Boundary conditions used for the 3D calculation.....	25

Figure 22 Bilinear interpolation method in 3D model.....	27
Figure 23 Equation setting of meshed 3-dimensional model in Elmer program.....	27
Figure 24 Surface potential on 1-mm thick PMMA disc at (a) 0 [h], (b) 3 [h], (c) 6 [h],	28
Figure 25 Surface potential on 2-mm thick PMMA disc at (a) 0 [h], (b) 3 [h], (c) 6 [h],	29
Figure 26 Surface potential on 10-mm thick PMMA disc at (a) 0 [h], (b) 3 [h], (c) 6 [h],	30
Figure 27 Surface potential decay with time on (a) 1-mm, (b) 2-mm, and (c) 10-mm thickness.....	31
Figure 28 Estimated surface charge density on 1-, 2- and 10-mm thick PMMA at 0 [h]	31
Figure 29 Calculated potential on (a) 1-, (b) 2-, and (c) 10-mm thick PMMA disc at 0[h]	32
Figure 30 Electric field in the z-direction for 1-, 2- and 10-mm thick PMMA at 0 [h]..	33
Figure 31 Surface charge density calculated by FEM of 1-, 2- and 10-mm thick PMMA at 0 [h].....	33
Figure 32 3D calculated potential of 1-, 2-, and 10-mm thick PMMA disc at 0 [h].....	34
Figure 33 Simulation result of surface potential in GiD program.....	35
Figure 34 Calculated charge density on a 1-mm thick PMMA disc at 0-3 hours.....	35
Figure 35 Calculated charge density on a 1-mm thick PMMA disc at 3-6 hours.....	36
Figure 36 Calculated charge density on a 1-mm thick PMMA disc at 6-24 hours.....	36
Figure 37 Calculated charge density on a 2-mm thick PMMA disc at 0-3 hours.....	37
Figure 38 Calculated charge density on a 2-mm thick PMMA disc at 3-6 hours.....	37
Figure 39 Calculated charge density on a 2-mm thick PMMA disc at 6-24 hours.....	38
Figure 40 Calculated charge density on a 10-mm thick PMMA disc at 0-3 hours.....	39
Figure 41 Calculated charge density on a 10-mm thick PMMA disc at 3-6 hours.....	39

Figure 42 Calculated charge density on a 10-mm thick PMMA disc at 6-24 hours.....	39
Figure 43 Data files in case of 1-mm thick PMMA disc calculated from ElmerGUI.....	45
Figure 44 Display Data tap for selecting the TXT file.....	46
Figure 45 Display Text Import Wizard for selecting “Delimited”	46
Figure 46 Display Text Import Wizard for selecting “Tab” and “Space”	47
Figure 47 Display a spreadsheet of nodes data	47
Figure 48 Display Import Data a tap for selecting the xls file	48
Figure 49 Display Import section for selecting the output type of “Numeric Matrix”. ..	48



CHAPTER 1

INTRODUCTION

1.1 General introduction

The high voltage is widely used for the transmission of electric energy. The principal reason that electric power is usually transmitted at high voltage levels is to increase efficiency. As electricity is transmitted over long distances, the energy losses are reduced by the high voltage usage, which results in the lower current. The high voltage transmission lines and associated equipment need appropriate insulation for operation safety. The insulation is done by using dielectric materials, which have low electric conductivity and can withstand high electric field stress. There are several types of dielectric materials such as gas, liquid, and solid materials. Solid materials are widely used for insulation in high voltage systems. The solid insulator must be mechanically strong enough for the purpose of support and separation. For example, in high-voltage transformers, solid insulation provides mechanical rigidity, while oil or other liquid dielectric materials contribute to primary insulation and serve to dissipate heat from the equipment. Dielectric materials play an important role in electronic circuits such as capacitors or insulators. In addition to high-voltage application, solid dielectrics are widely used for power-electronic equipment. It is important to note that the insulation performance of solid dielectrics can be decreased by the electrical charges on the surface of materials.

In the worst case, electrostatic discharge (ESD) resulted from surface charges may cause industrial hazards such as the occurrence of fire or explosion. The effects of surface charges on dielectric materials also gain attention due to another reason. Recently, the utilization of high voltage direct current (HVDC) transmission is increasing. DC high voltage is simple to use and available as generated from renewable energy resources. Under HVDC, it is easy to charge the surface of solid dielectric materials. Therefore, it is essential to understand physical phenomena related to surface charging. This includes the charge-relevant process of surface acrylic or polymer of methyl methacrylate (PMMA). The material is in popular use as a good electrical insulator.

This thesis studies on the temporal decay of surface charge on a dielectric material. PMMA sheets of different thickness are used as the samples. The dielectric sheet surface is charged by DC corona discharge under low to medium humidity environment (absolute humidity between 5 and 10 g/m³). The surface charge decay will be investigated for different conditions of PMMA thickness. Three mechanisms of charge decay process will be considered. Numerical simulation will be carried out to analyze the experimental results. The factors that affect the surface charge decay on the PMMA surface are then concluded.

1.2 Literature review

There are a number of experimental and analytical works on the reduction of surface charge potential. Both simulation and measured results have been reported. Moreover, the knowledge from the works of literature have expressed the mechanism of the surface potential decay.

J. Kindersberger et al. focused on the simulation part of surface charge decay on insulator in air and SF₆ [1]. This paper presented the surface charges decay on polymeric insulators in air and SF₆. Three mechanisms of charge decay were investigated. The corona discharge was simulated on the polymeric insulator surface. The simulation and theory of charge decay were treated in this paper.

Physical mechanisms were the cause of the surface charge reduction. The electrical conduction through the volume of the insulator, the electrical conduction along the surface of the insulator and the charge neutralization by gas ions were referred to explain the reduction of surface charge. The simulation model was computed by using a software based on the finite element method (FEM). The surface charge distribution density was calculated based on the measured results from the charging process of the rod-plane electrode. A rotational symmetry model was used to analyze the surface charge density. According to the insulator thickness, the surface potential distribution decreased with time. The ionization current density depended on electric field strength. The current density increased linearly at the low electric field strength before it was steady. Although the ionization current density both in air and SF₆ followed exponential trend, the

current density of SF_6 was lower than that in the case of ambient air. The reduction of surface charge was due to the mentioned mechanisms. Each mechanism affected differently the decay of surface charge distribution. The conduction through the isolation volume reduced overall the surface charge distribution with elapsed time. The mechanism of conduction through the insulator surface reduced the surface charge at the border and spreaded the charge in the radial direction.

The profile of surface charge potential modified by charge neutralization gas ions was similar to a crater shape. The surface potential distribution decreased remarkably at the center. Under DC voltage, the distributions of the surface charge on the cone-type spacer concave were similar for different voltage amplitudes. The surface charge accumulation was dominated by the electric conduction through the volume. The peak value of the surface potential on the spacer increased linearly with the residual DC voltage amplitude.

J. Kindersberger et al. explained the surface charge decay measured on insulator in air and SF_6 [2]. The three mechanisms were used to explain the characteristic of surface potential distribution. The surface charge was generated on the surface of insulators which made of polytetrafluorethylene (PTFE), silicone rubber (SIR), and epoxy-resin (EP).

In the experiment, a needle-plate electrode system was used to generate the corona discharge. A circular plate of the insulator was located on a plane electrode which was grounded. The test was done in ambient atmospheric air and SF_6 . Although the rod to plane electrode was similarly used to generate the surface charge, the SF_6 experiment was done in a pressurized vessel. The surface charge potential was measured by a probe which was connected to an electrostatic voltmeter. The surface charge density was then calculated from the surface potential distribution. Normally, the surface charge potential distribution should be a symmetry bell-shape. Note that an object in the proximity of the charged surface may affect the surface potential by charge neutralization by gas ions. The measurement for epoxy-resin was done close to a cross table. Therefore, the measured results of surface charges on an epoxy-resin were distorted.

Their surface charge distributions were bell-shaped. The surface potential distribution on silicone rubber decayed overall with time. In addition, the surface potential distribution of epoxy-resin and PTFE were initially bell-shaped. Then, it decreased to take a crater shape. In the case of SF₆, only the PTFE was used. The reduction of surface potential distribution expressed the crater shape which was explained as a result from charge neutralization by ambient gas ions. The measured results reveal that the material of the solid insulator, the surrounding gas, and the charged area influenced the reduction of surface potential distribution. In the case of enclosed-area, particularly GIS, the charge neutralization by gas ions plays an important role in the characteristic of charge decay.

T. Matsumoto et al. presented the investigation and numerical analysis of surface charge decay on acrylic and glass epoxy having multilayer structures in air [3]. The DC corona discharge was constructed by using a rod to plane electrode system and a DC power supply. In the case of positive DC corona, the rod electrode was connected to the DC voltage. The plane electrode was connected to ground. The opposite connection was applied in the negative corona case. The plane electrode was overlaid by a dielectric disc which was an acrylic and glass epoxy multilayer. The room temperature and humidity were controlled by an air conditioner. The surface charge potential was automatically measured by a scanning probe which was connected to an electrostatic voltmeter.

In the case of positively or negatively charged acrylic disc, the measured temporal surface potential was bell-shaped initially. The peak value of the initial surface potential of the positive case was higher than the negative one. Then, the surface potential distribution decayed into a crater shaped. In the simulation part, the surface charge decay on the acrylic surface was estimated by using the experimental condition. The charge simulation method was used to calculate the electric field distribution along the acrylic surface. The surface potential distributions were indicated at 24, 48, and 72 hours, respectively. It was shown that the simulation results and the measured results were similar in the case of the acrylic. In the case of a glass epoxy multilayer disc, the experiment was done only

with the positive DC corona discharge. The peak value of the initial surface potential was lower than the acrylic. Although the potential distribution was bell-shaped, as same as the case of acrylic, the trend of surface charge decay was faster than the acrylic. In the case of acrylic, the surface potential distribution decreased like a crater on elapsed time. The main reduction mechanism of surface potential is due to the charge neutralization by gas ions. In the case of glass epoxy multilayer, it has low volume resistivity. Hence, the electric conduction through the volume apparent into the charge neutralization.

Q. Du et al. studied the surface charge distribution on DC basin-type insulator [4]. The aim of this paper was to study the surface charge distribution on DC basin type insulator, especially for the gas-insulated transmission line (GIL). The SF₆ gas was filled in a GIL chamber where the insulator was located. The surface charge measurement device was connected to the GIS transfer unit. The measurement system consisted of a mechanical device for moving a probe, a HV shielding system and a control system. The HV shielding was used to install the conductor of the basin-type insulator.

In the experiment, the bushing linked high-voltage direct current (HVDC) generator and the GIS transfer unit as shown in figure 1. The programmable logic controller (PLC) was written for the probe movement based on the insulator shape in the measurement system. The experiment results were the charge distribution under DC voltage. The surface potential distribution was symmetrical circular shape under condition of voltage polarity influence (+80 and -80 kV). For +120, +160 and +200 kV, the increase of voltage amplitude caused the accumulation of charge at certain areas on the insulator surface. The surface charge was reduced by gas neutralization, surface conduction, and bulk conduction. The gas-side normal electric field and gas conduction mechanism were used to explain the potential distribution.

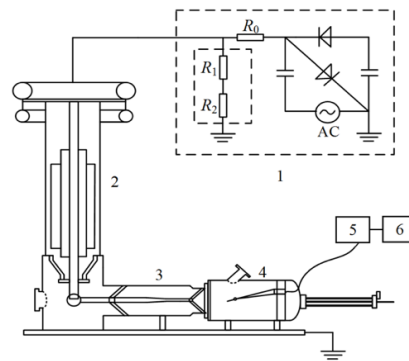


Figure 1 Experiment setup (1-HVDC generator, 2-Bushing, 3-GIS transfer unit, 4-Surface charge measurement device, 5-Charge amplifier, 6-Data acquisition system) [4]

H. Zhou et al. focused on the surface charge accumulation on 500kV cone type GIS spacer under residual DC voltage [5]. The cone-type spacer was the main component of GIS. In this paper, the spacer was studied for a full-scale surface charge measurement platform. The DC voltage experiments were done to investigate the surface charge distribution on the spacer. The experimental conditions were difference in voltage amplitude and DC electric stress.

The experimental setup consisted of gas-insulated bus bars (GIB) 500kV, cone type spacer, 4-axis handling system, and measurement device. The experiment was done in a vacuum chamber which was filled with the SF_6 gas. The DC voltage was applied to the cone-type spacer. In the measurement, the probe was connected to the four-axis handling system which including sliders, stepper motors, drives, and controllers. The experimental results were illustrated as the surface potential under DC voltage of -50, -100 and -150 kV. The surface potential was measured at 20, 40, and 60 hours after applying the voltage. The initial electric field in the spacer under negative polarity condition was used to explain that the surface charge distribution was dominated by the mechanism of charge decay. The reduction was governed by the electrical conduction through the volume of the insulator. The results revealed that the charge accumulated was highest on the middle area of spacer.

C. Li et al. reviewed the literature about the surface charge accumulation of surface flashover on spacers in compressed gas insulation [6]. The study and review of relevant kinds of literatures was proposed to analyze the problem directly. The review showed that the surface flashover was affected by the materials of insulation, electrodes, voltage waveform, and geometries. The surface charge accumulation under DC voltage had become prominently. The charge accumulation or injection on the insulator surface played an important role in compressed air. Therefore, the surface charge accumulation and polymer insulation materials were studied by many researchers.

The factors that affected the surface charge distribution included the shape of an insulator, electrode, applied voltage and polarity, temperature, humidity, and dielectric surface. C. N. Cooke studied the charging of insulator surfaces by ionization and transport in gases [7]. Cooke presented that the surface charge accumulation appeared when the rate of charge arrival exceeded the surface charge conduction rate. The surface charge accumulation on the surface occurred when the discharge appeared nearby. Therefore, it can be explained that the charge related to a particular nearby source. The charge was influential by the fields at the source region and by the emission from the layer of insulator. In the experimental section, the post-type epoxy insulator was used for the test arrangement. It was found that the amount of charge accumulated on the insulator from a nearby source. Researchers studied the surface charge accumulation with different type of spacer. Different types of spacer model were identified. K. Nakanishi presented the surface charging on epoxy spacer at DC stress in compressed SF₆ gas [8]. The results were based on the experiment of cylindrical, post and conical epoxy spacers. The charge accumulation on the model was measured by using the electrostatic probe and observed the accumulated charge by using the dust figure technique. Only a conical model, the rough and fine finish conductor was used in the experiment. The rough one was used with negative polarity in DC. The negative charge was accumulated on a concave side. In the case of fine finish conductor, the hetero charge was appeared on the concave surface.

1.3 Objectives of the thesis

1.3.1 To study the surface charge accumulation and reduction on the dielectric materials

1.3.2 To investigate the dependency of charge decay and its mechanisms on the specimen thickness

1.4 Scope of the thesis

1.4.1 The study is limited to the surface charge reduction on the surface of the PMMA for different thickness.

1.4.2 The distribution of potential, electric field, and surface charge were determined by the finite element method (FEM).

1.5 Expected outcome

1.5.1 Clarify the relationship between the surface potential and the charge distribution

1.5.2 Understand the mechanism of charge reduction on solid insulator

CHAPTER 2

THEORY

In the thesis, the numerical simulation is applied for calculating the surface charges on the PMMA samples. The simulation is based on the measured results. The electric potential is to be calculated by using the 2-dimensional axisymmetric and 3-dimensional finite element method (FEM).

2.1 Discharge and accumulation of charges

Air is normally used as the insulation for power systems. Both applied voltage and gap distance are the main conditions for the breakdown in the air. The gas ionization under the effect of an electric field causes electrical discharge. The applied voltage waveform and the gap geometry are the external conditions that define the variation and distribution of the electric field. The electrical discharge is caused by the ionization of the surrounding gas, generating luminous plasma. It produces electrical and thermal physical phenomena and then finally results in the breakdown in the gap. Corona discharge exhibits the luminescent and thermal phenomena due to the gas ionization and recombination processes. The luminous layer due to corona discharge is generated near the electrode before the breakdown of an air gap. The corona onset voltage is lower than the breakdown voltage as the corona discharge mitigates the distribution of the electric field. The surface charge accumulation can occur under DC corona discharge. There are many mechanisms that can lead to the transfer of electrostatic charges from conductor to insulators. The surface charge accumulation may affect the initiation and propagation of discharge. In normal conditions, the breakdown voltage for negative is higher than the positive polarity. Therefore, the long air gap discharge characteristics under positive polarity are considered for insulation coordination [9].

2.2 Electric field simulation

The electric field simulation [10] is used to analyze the surface charge distribution. The electric field can be calculated from the electric potential, which is the solution of the Poisson's equation. Boundary conditions are used to determine the

electric potential. The electric potential is used to calculate the electric field. The electric field \mathbf{E} is related to the electric potential ϕ by

$$\mathbf{E} = -\nabla\phi \quad (1)$$

A 2-dimensional (2D) model and a 3-dimensional (3D) model are used to calculate the electric potential and electric field. From equation (1), the equation can be written the composition of \mathbf{E} in the cylindrical coordinate system to use for the axisymmetrical calculation is

$$\mathbf{E} = -\left(\frac{\partial\phi}{\partial\rho} + \frac{\partial\phi}{\partial z}\right) \quad (2)$$

$$\mathbf{E} = E_\rho \mathbf{a}_\rho + E_z \mathbf{a}_z \quad (3)$$

In the case of three-dimensional calculation, the composition of \mathbf{E} in the cartesian coordinate system is formed as

$$\mathbf{E} = -\left(\frac{\partial\phi}{\partial x} + \frac{\partial\phi}{\partial y} + \frac{\partial\phi}{\partial z}\right) \quad (4)$$

$$\mathbf{E} = E_x \mathbf{a}_x + E_y \mathbf{a}_y + E_z \mathbf{a}_z \quad (5)$$

where \mathbf{E}_ρ and \mathbf{E}_z are the electric field in the direction of ρ and z , respectively. \mathbf{a}_ρ and \mathbf{a}_z are the unit vector in the direction of ρ and z . In the system of 3-D cartesian coordinate, \mathbf{E}_x , \mathbf{E}_y and \mathbf{E}_z are the electric field in the direction of x , y and z , respectively. \mathbf{a}_x , \mathbf{a}_y and \mathbf{a}_z are the corresponding unit vectors. Electric flux density \mathbf{D} is a vector field related to the electric field \mathbf{E} . The relationship between \mathbf{D} and \mathbf{E} is

$$\mathbf{D} = \epsilon_0 \epsilon_r \mathbf{E} \quad (6)$$

where ϵ_0 is the permittivity of free space = 8.854×10^{-12} F/m, and

ϵ_r is the dielectric constant.

The electric field is composed of normal and tangential components. The flux density \mathbf{D} can be written as

$$\mathbf{D} = \epsilon_0 \epsilon_r (\mathbf{E}_\rho \mathbf{a}_\rho + \mathbf{E}_z \mathbf{a}_z) \quad (7)$$

The subscripts ρ and z indicate the direction in the cylindrical coordinate. The surface charge density σ_s is defined as the total outward flux per surface area. The electric field in the ρ -direction is parallel to the PMMA surface. Hence, the field in z -direction was used to calculate the surface charge density.

$$\sigma_s = \epsilon_0 \epsilon_{r1} E_{z1} - \epsilon_0 \epsilon_{r2} E_{z2} \quad (8)$$

where, the subscripts 1 and 2 correspond to the air and PMMA sides, respectively.

The flux density in the 3D cartesian coordinate system can be written as

$$\mathbf{D} = \epsilon_0 \epsilon_r (\mathbf{E}_x \mathbf{a}_x + \mathbf{E}_y \mathbf{a}_y + \mathbf{E}_z \mathbf{a}_z) \quad (9)$$

The field in the y -direction was used to calculate the surface charge density see figure 2.

$$\sigma_s = \epsilon_0 \epsilon_{r1} E_{y1} - \epsilon_0 \epsilon_{r2} E_{y2} \quad (10)$$

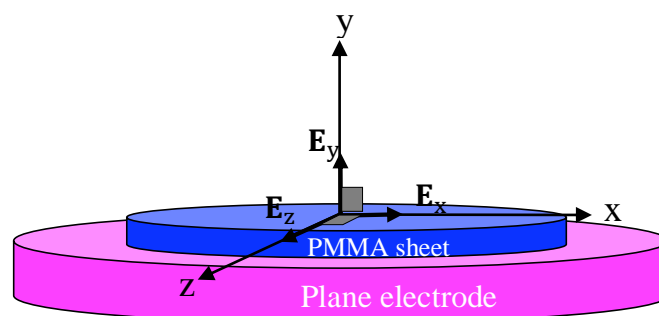


Figure 2 3-dimensional model of PMMA sheet placed on plane electrode

2.3 Finite element method (FEM)

For typical numerical field calculation methods, domain and boundary geometries must be modeled. For the FEM, the domain of calculation is discretized into small portions called elements. Interpolating functions, often called shape functions, are used to estimate quantities such as the shape of element, potential, electric field, or charge density, etc. The approximation of element that transforms the actual coordinates to and from local coordinates is constructed. Conformal interpolation using nodal values is in the form [11-13]

$$\phi = \sum_{i=1}^n N_i \phi_i \quad (11)$$

where ϕ is the quantity to be interpolated, ϕ_i is the quantity at node i , and N_i is the interpolating function associated with node i . This research uses the triangular and rectangular elements in the system of 2-dimensional (2-D) and then uses the tetrahedral element in the system of 3-dimensional (3-D). The first order triangular element consists of three nodes and three sides as illustrated in Figure 3.

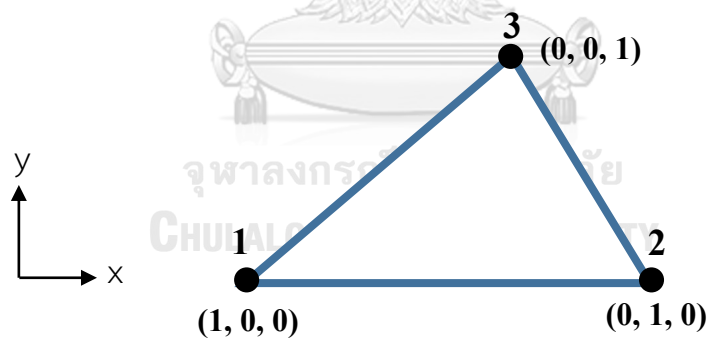


Figure 3 Triangular element

The formulas for the shape functions of triangular are in terms of L_1 , L_2 , and L_3 that are given by

$$N_1 = L_1 \quad (12)$$

$$N_2 = L_2 \quad (13)$$

$$N_3 = 1 - L_1 - L_2 \quad (14)$$

where L_1 , L_2 , and L_3 are the local coordinates which are between 0 and 1, and $L_1 + L_2 + L_3 = 1$ for the triangular element. The first order rectangular element is a 2-D finite element consists of four nodes and four sides as shown in Figure 4.

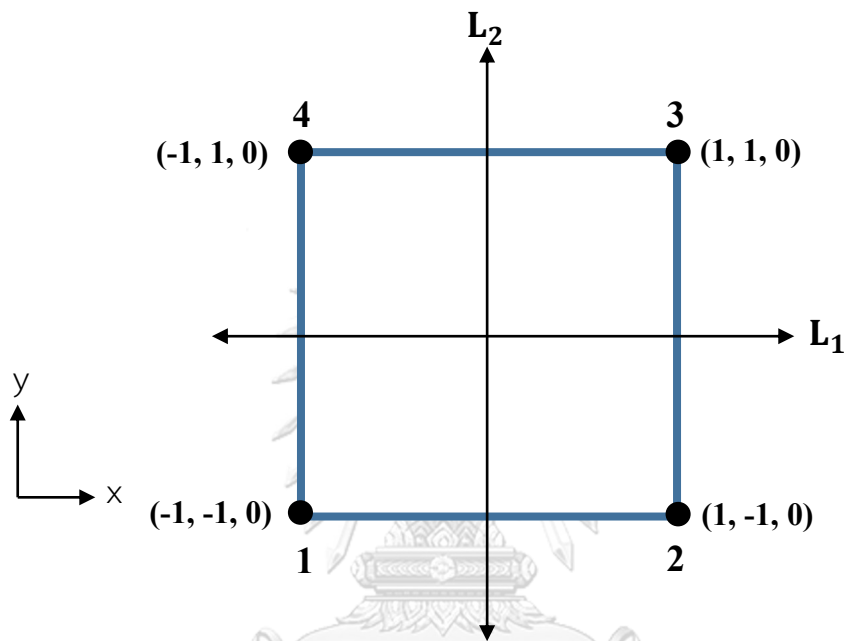


Figure 4 Rectangular element

The formulas for the shape functions of rectangular are in terms of L_1 , L_2 , and L_3 where L_1 , L_2 are the specific point which have a value between -1 and 1.

$$N_1 = \frac{1}{4}(1 - L_1)(1 - L_2) \quad (15)$$

$$N_2 = \frac{1}{4}(1 + L_1)(1 - L_2) \quad (16)$$

$$N_3 = \frac{1}{4}(1 + L_1)(1 + L_2) \quad (17)$$

$$N_4 = \frac{1}{4}(1 - L_1)(1 + L_2) \quad (18)$$

The first order tetrahedral element is a 3-D finite element consists of four nodes and four sides as shown in Figure 5.

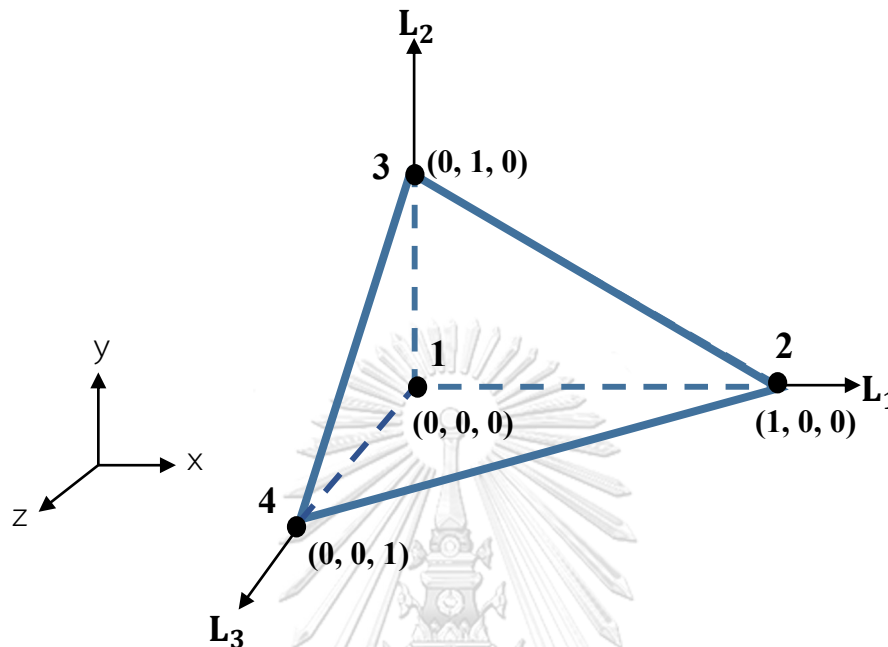


Figure 5 Tetrahedral element

The formulas for the shape functions of tetrahedral are in terms of L_1 , L_2 , and L_3 that are given by

$$N_1 = L_1 \quad (19)$$

$$N_2 = L_2 \quad (20)$$

$$N_3 = L_3 \quad (21)$$

$$N_4 = 1 - L_1 - L_2 - L_3 \quad (22)$$

where L_1 , L_2 , and L_3 are the local coordinates which are between 0 and 1, and $L_1 + L_2 + L_3 = 1$ for the tetrahedral element.

CHAPTER 3

EXPERIMENT

The experimental procedure is important to study the surface potential distribution. The author did experiment for determine the potential, electric field, and surface charge density on the different condition of dielectric thickness.

3.1 Experimental method

1-, 2- and 10-mm thick PMMA sheets were stored in a desiccator ($\approx 40\text{-}55\%$ RH) before use in the experiment. The upper and lower surface of PMMA discs were cleaned by using ethyl alcohol. As shown in the figure 6, the example of 1-mm thick PMMA disc was prepared to use in the experimental procedure. And then the sample sheets were preconditioned by using a static eliminator (495, HAKKA) to reduce static electricity, as shown in figure 7.

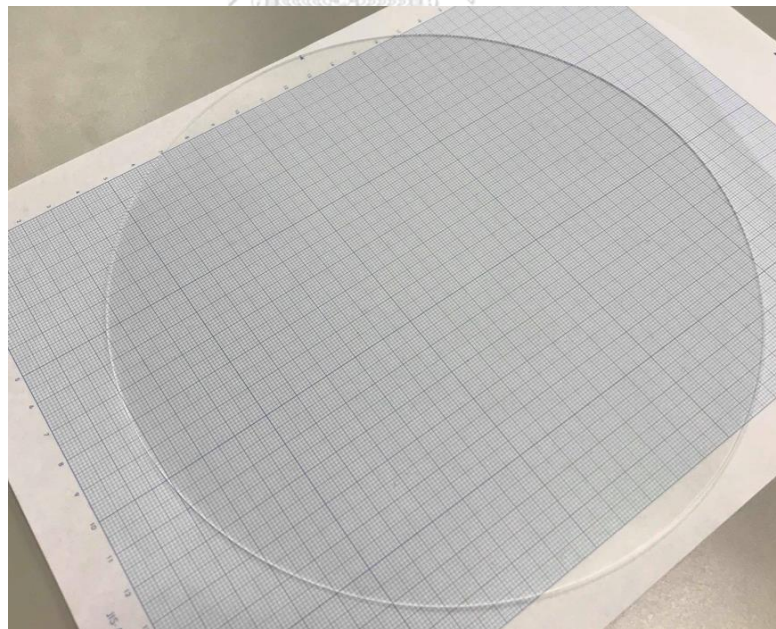


Figure 6 1-mm thick PMMA disc



Figure 7 Static eliminator (495, HAKKA)

In the experiments, a rod-plane electrode configuration was used to generate the corona discharge on the PMMA surface. The experimental setup included a DC high-voltage supply (DCG-100KITS, No. 6011-2), and a digital Multimeter (VOAC 7413, IWATSU), as illustrated in figure 8.

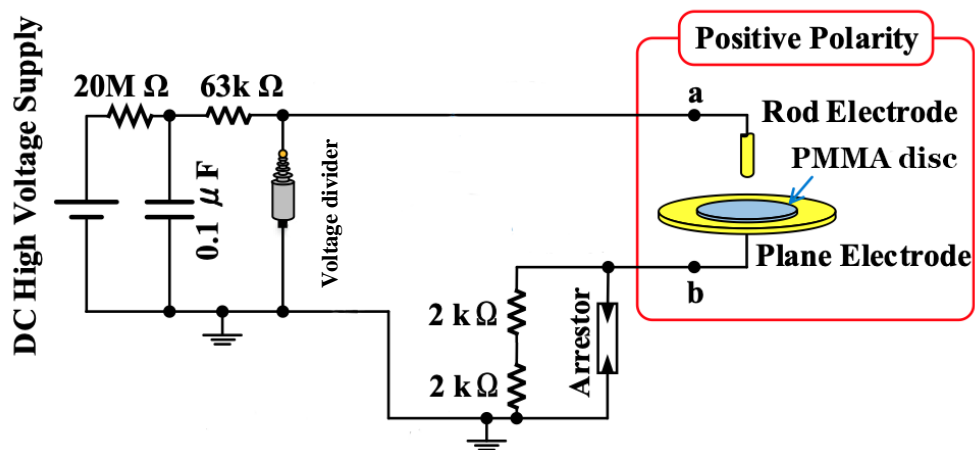


Figure 8 Schematic drawing of experiment setup [14]

In the experimental setup, the 20-M Ω is the protective resistance for the power supply. The 63-k Ω is used as a ballast resistance which controls the amount of current for preventing breakdown. The capacitors are used to stabilize the DC voltage.

The 0.3-cm diameter rod electrode was connected to the DC supply voltage. The plane electrode of 35 cm diameter was grounded. PMMA samples of 1-, 2-, or 10-

mm thickness of (diameter of 20 cm.) were placed on the plane electrode. The gap distance between rod and plane electrode was 2 cm as shown in figure 9. The amplitude of applied voltage was increased to 13.0 kV and sustained for 5 minutes. The experiments were done in a laboratory where the temperature was about 20°C. The humidity was in the low to medium level (absolute humidity between 5 and 10 g/m^3).

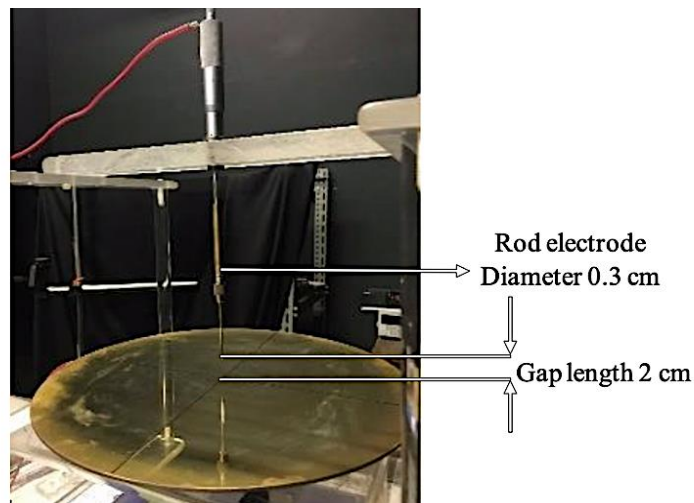


Figure 9 Rod-plane electrode configuration

3.2 Measurement procedure

The surface potential on the PMMA disc surface was measured under the same temperature as that during the experiment. The room temperature was set at 20°C by using the air conditioner. The surface potential was measured with elapsed time t [h].

The measuring system included an electrostatic voltmeter (542, TREK), a scanning probe (542P-S, TREK), a stage controller (SHOT-202, Sigma Koki), and an X-Y stage. The probe was connected to the electrostatic voltmeter for measuring the surface potentials on the PMMA surface. The PMMA disc placed on the plane electrode was automatically moved together by the XY-stage. The principle of the measurement system was arranged, as shown in figure 10. The surface potential was recorded with 5 mm resolution. The gap between probe and PMMA sheet was about 6 mm, as shown in figure 11.

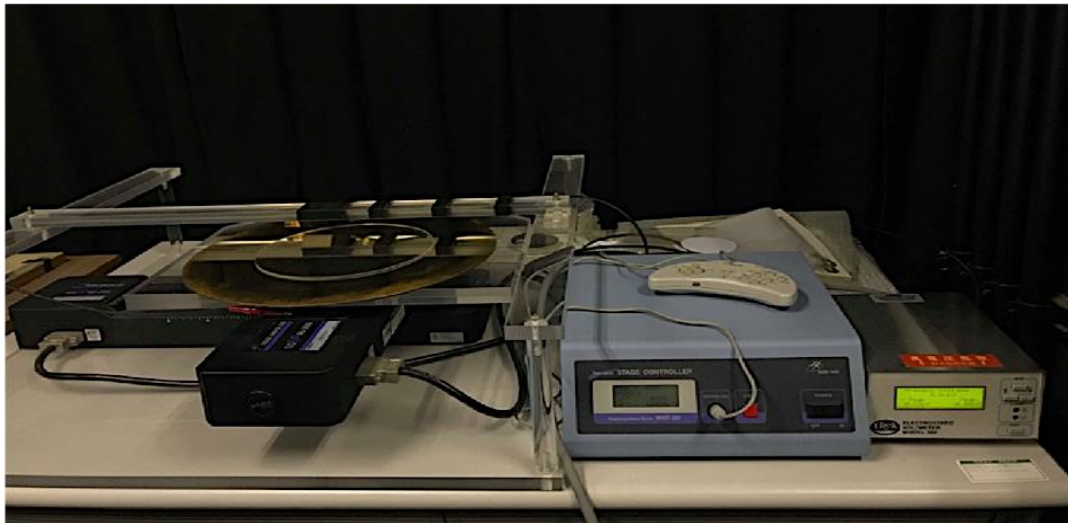


Figure 10 Measurement system

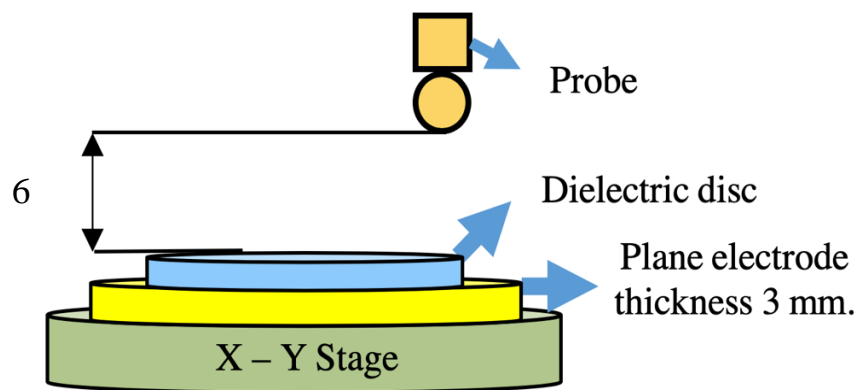


Figure 11 Configuration of surface charge measurement

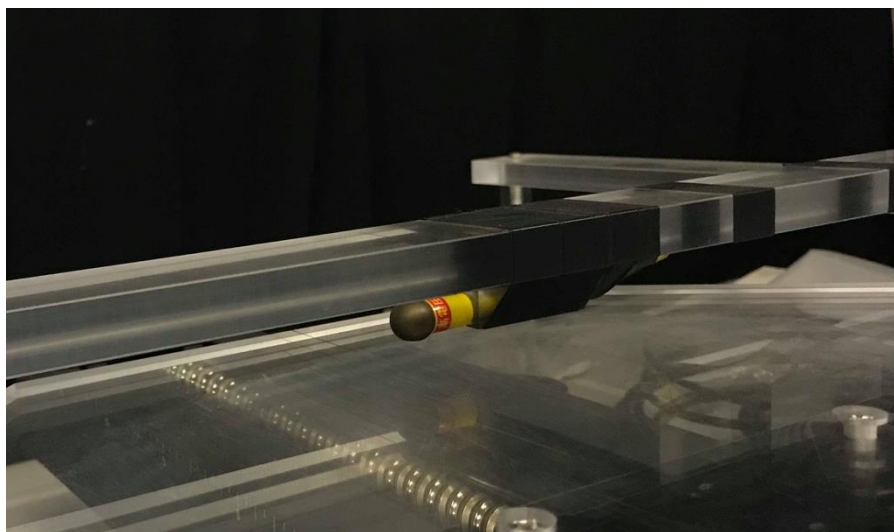


Figure 12 Measurement probe

The surface potential was measured from 0 to 24 hours after applying voltage. The experiments gave the distribution of surface potential of 1-, 2- and 10-mm thick PMMA.

CHAPTER 4

SIMULATION

This chapter describes the simulation models that were executed in an FEM program, Elmer. The surface potential was applied as the boundary condition on the insulator surface. The geometries were modeled with the GiD program. The 2D and 3D simulation models are used to calculate the surface potential and then electric field by using the Elmer program.

4.1 2D simulation

The 2D axisymmetric simulation model was created with the GiD program is shown in figure 13. The domains were subdivided to triangular and rectangular elements in GiD, as illustrated in figure 14. The materials and boundary conditions according to the measurement condition were used. Surface potential condition in 2D model was determined as follows.

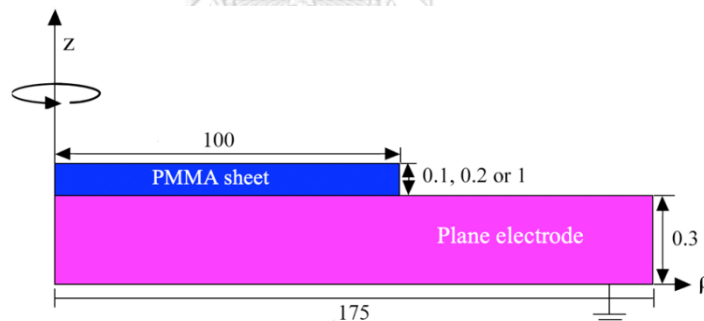


Figure 13 2-dimensional axisymmetric models (dimensions are in mm.)

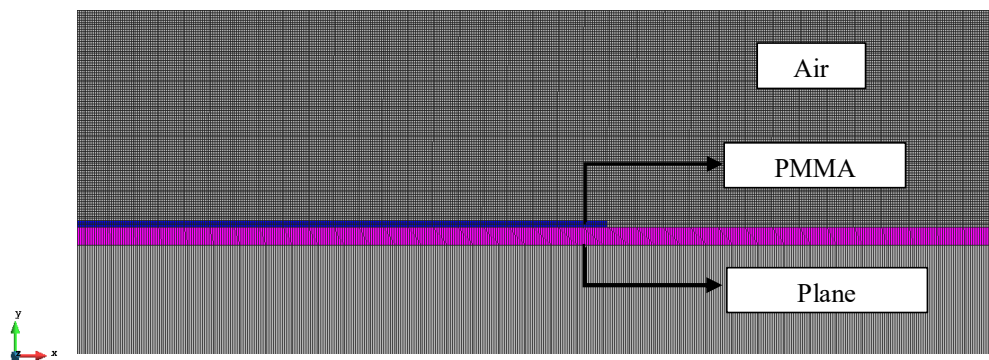


Figure 14 Meshed 2-dimensional model through the GiD program

The setup boundary condition of potential in PMMA surface was calculated by using interpolation method to estimate the potential values that lie between two nodes. The formula of linear interpolation is

$$p_i = p_1 + (x_i - x_1) \frac{(p_2 - p_1)}{(x_2 - x_1)} \quad (23)$$

where x_1 and x_2 are the coordinates at the node 1 and 2,

p_1 and p_2 are the potential values at the node 1 and 2,

x_i is the known x -coordinate to perform the interpolation,

and

p_i is the interpolated potential value.

The measured surface potential was recorded in each 0.5 cm position. Figure 15 shows the PMMA disc displayed in a 0.5-centimeter grid view. The known values from collected data points nearest to x_i were selected to calculate the interpolation potential p_i . For 1D interpolation, the parameter of x -coordinates and potential values were chosen as variables in the formula.

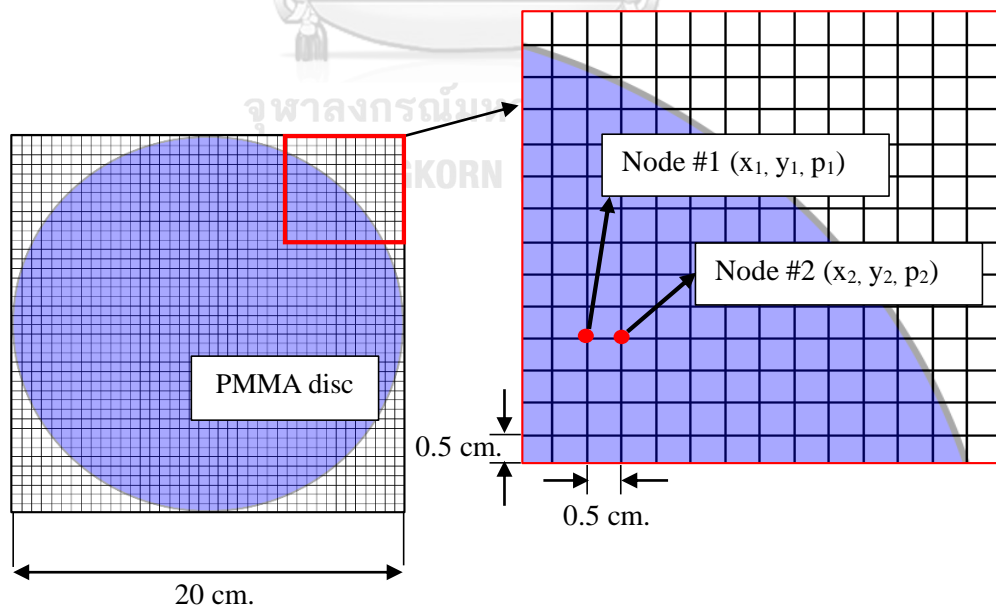


Figure 15 Division of the PMMA disc in 0.5-centimeter grids

Figure 16 shows the example of 1D interpolation of potential p_i . x_1 and x_2 were the two known coordinate values, where $x_1 < x_i < x_2$. y -coordinates were set constant as a $y=0$ line. x_1 (the first node) and p_1 (its potential value) are 0 and 3.6288, respectively. x_2 (the second node) and p_2 (its potential value) are 0.5 and 3.5442, respectively. x_i that lied between two nodes is 0.25. Then, we calculate

$$p_i = 3.6288 + (0.25 - 0) \frac{(3.5442 - 3.6288)}{(0.5 - 0)}$$

$$p_i = 3.5865$$

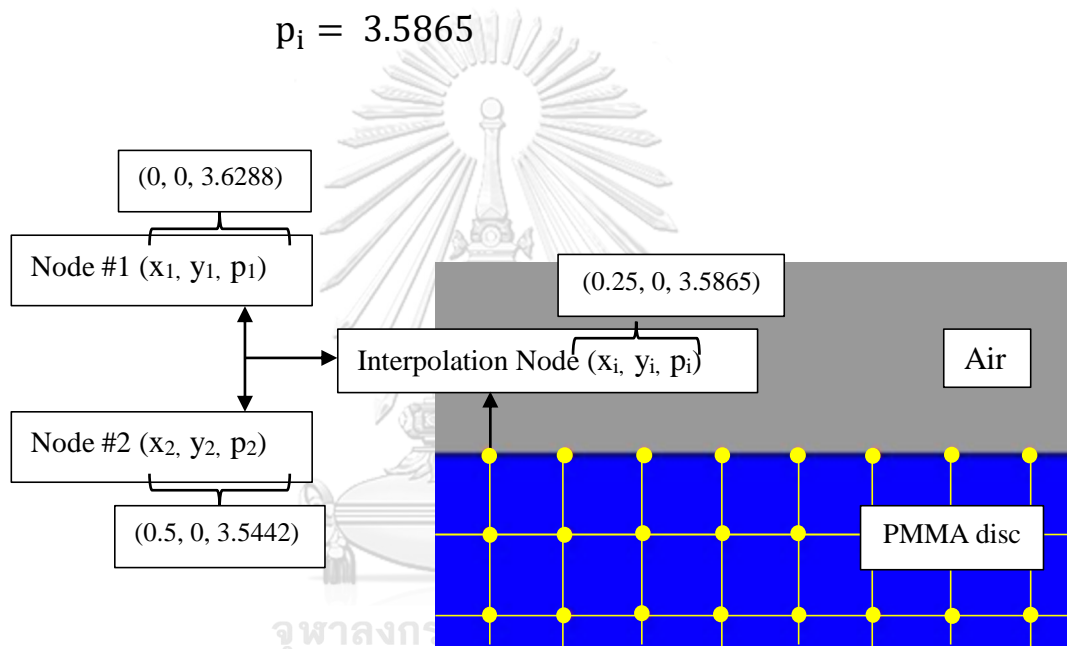


Figure 16 Linear interpolation for the 2D model

Equation (23) and data sets of measurement potential were coded in the Fortran90 language which was applied to the solver input file through Elmer GUI. In this case the file "calpotentialt1" was contained a shareable .dll (Windows) code for the user function whose name is "Calpotential". The call interface for the Fortran90 function is shown in figure 17.

The Elmer mesh file was provided a set of solvers, where was associated with the equation to solve a model. In the equation section, the electrostatic solver was assigned to the meshed model. In the solver-specific option, potential and electric fields were activated which were needed to invoke the computation. The screenshot

of the Elmer program is shown in figure 18. The potential values calculated in the Elmer program were saved as a file in Excel (.xls). The Excel files were imported into the MATLAB program which used to calculate the electric field and then surface charge density by the FEM.

```

Name = "Material 3"
Relative Permittivity = 1000
End

Boundary Condition 1
Target Boundaries(8) = 1 2 3 4 5 6 7 8
Name = "BoundaryCondition 1"
Electric Flux = 0
End

Boundary Condition 2
Target Boundaries(1) = 14
Name = "BoundaryCondition 2"
Potential = Variable Coordinate 1
Real Procedure "calpotential1 Calpotential"
End

Boundary Condition 3
Target Boundaries(4) = 17 19 22 23
Name = "BoundaryCondition 3"
Potential = 0
End

```

Figure 17 Sif file calling interpolating function for Elmer

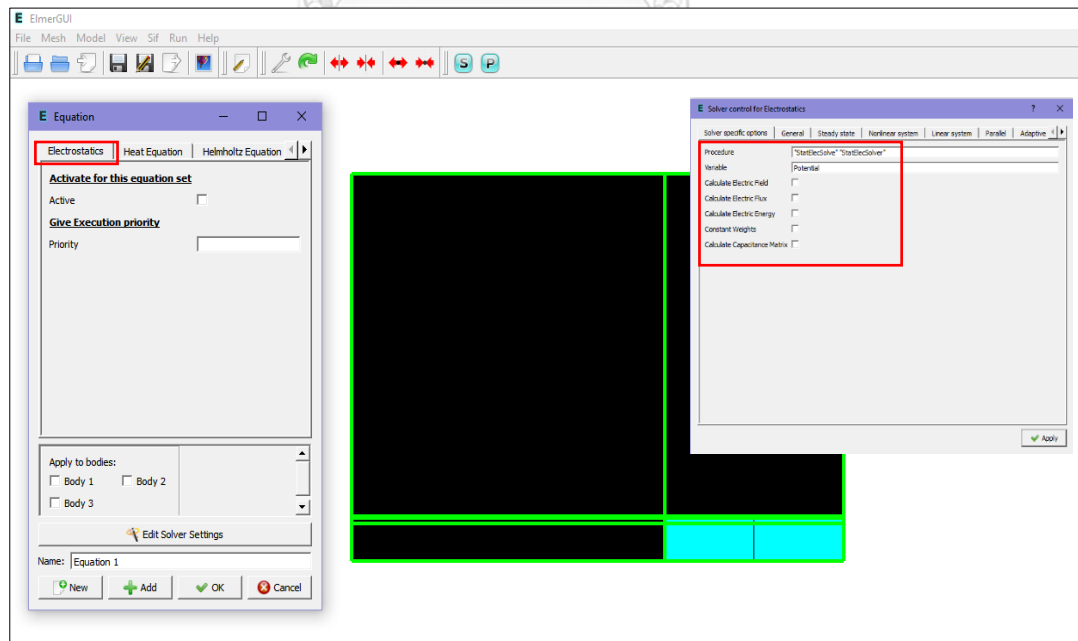


Figure 18 Setting for the 2-dimensional model in Elmer

4.2 3D simulation

The 3D simulation model was created by using a basic toolbox in the GiD program. The geometry of 3D model was created with tool of create line and arc. Then it was formed the surface and volume by using NURBS (Non-Uniform Rational B-Spline) function, as shown in figure 19. The configuration of simulation model based on experiment is shown in figure 20.

The type of materials on the model were categorized into air, PMMA and conductor of brass. The relative permittivity was used as the input variable to demonstrate the material properties. The boundary conditions were set as index numbers and then were represented with different colors, as shown in figure 21. The index numbers of 1 and 2 were defined to the interpolation potential in PMMA disc. The index numbers of 3 and 4 were defined to potential equal zero in plane electrode. The index numbers of 5 to 10 were defined to electric flux equal zero as the air-side walls.

The setup boundary condition of potential in PMMA surface was calculated by using 2D interpolation method. The interpolation method was performed the linear interpolation in x -axis, and then again in the y -axis.

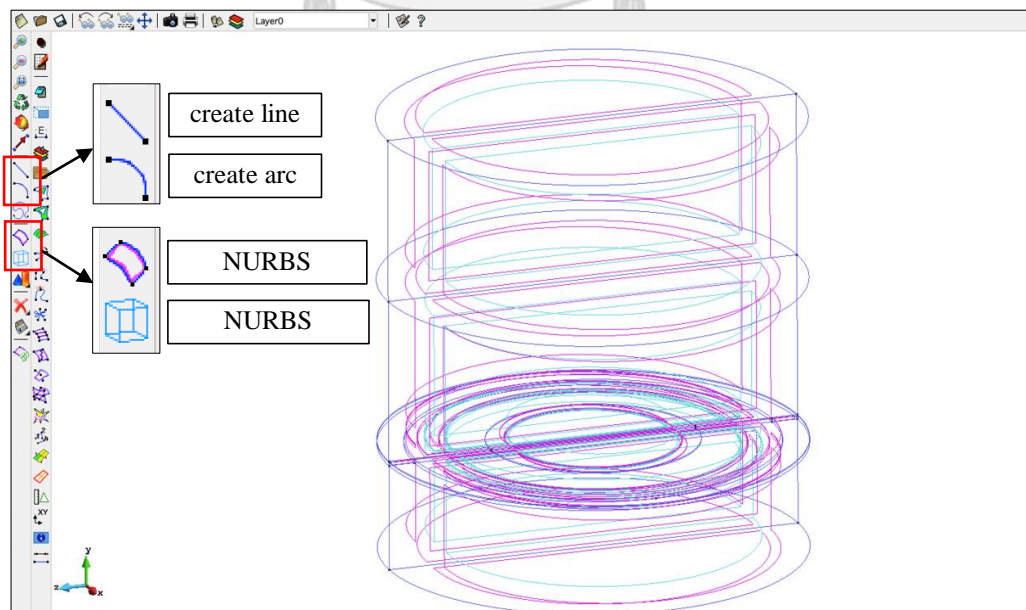


Figure 19 Geometry of 3D model and toolbox menu of GiD

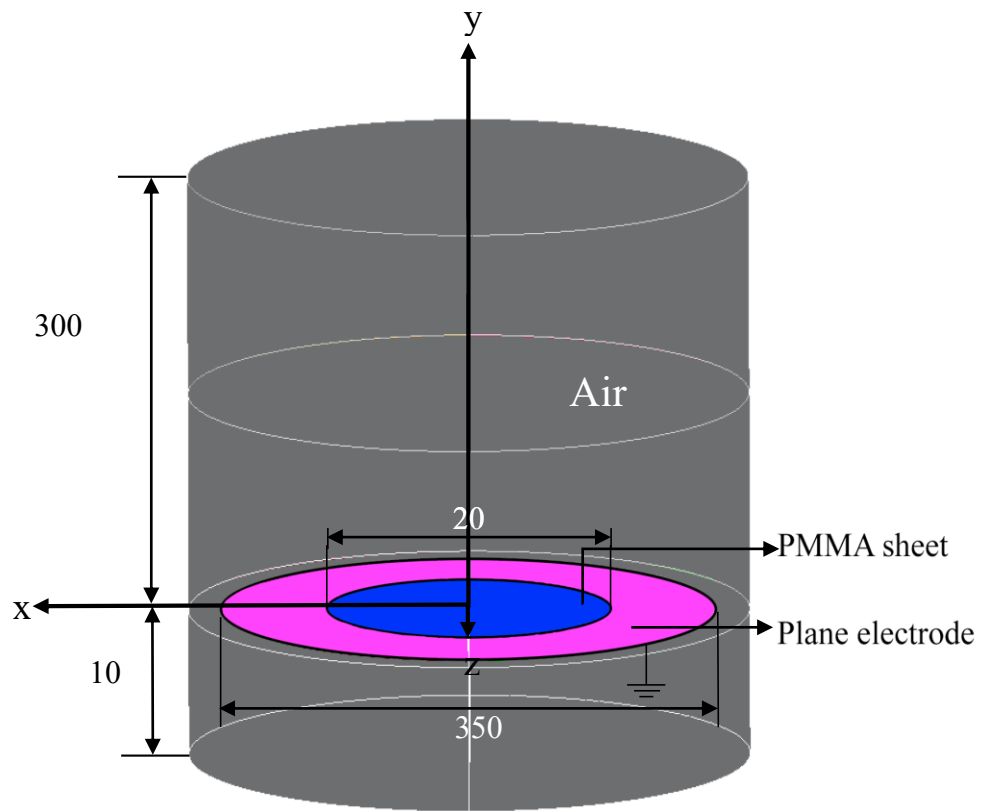


Figure 20 3D calculation model (dimensions are in mm.)

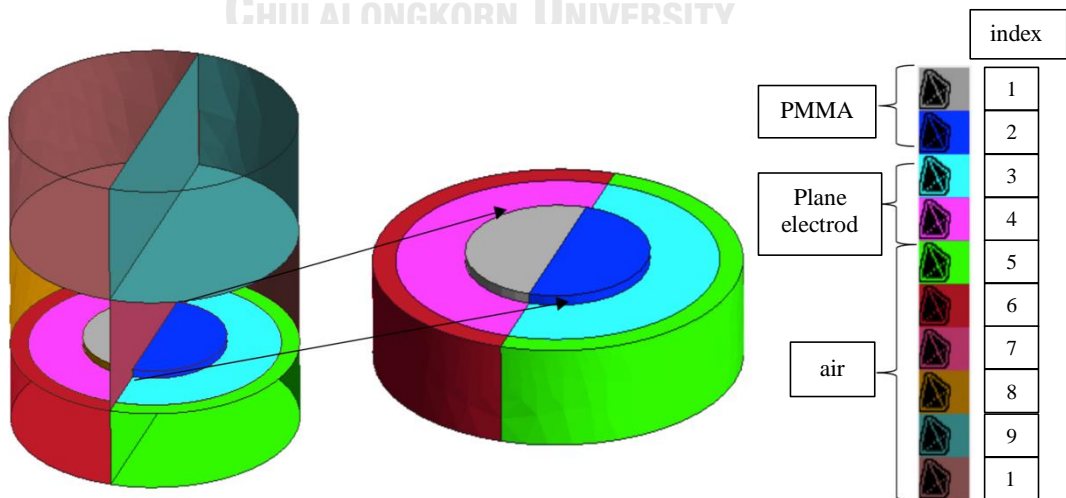
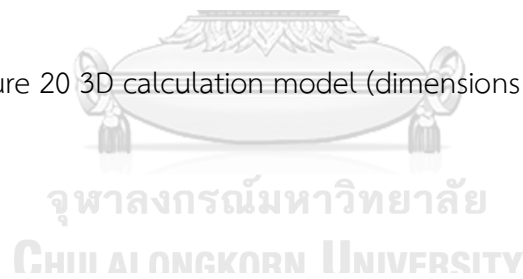


Figure 21 Boundary conditions used for the 3D calculation

Figure 22 shows an example of the interpolation for the 3D meshed-model using \mathbf{x} - \mathbf{y} pairs. The interpolation potential at $(\mathbf{x}_i, \mathbf{y}_i) = (0.25, 0.25)$ lies between four nodes. Assume that the coordinates at the four nodes are $(\mathbf{x}_1, \mathbf{y}_1, \mathbf{p}_1) = (0, 0, 3.6288)$, $(\mathbf{x}_2, \mathbf{y}_2, \mathbf{p}_2) = (0.5, 0, 3.5442)$, $(\mathbf{x}_3, \mathbf{y}_3, \mathbf{p}_3) = (0, 0.5, 3.6288)$, and $(\mathbf{x}_4, \mathbf{y}_4, \mathbf{p}_4) = (0.5, 0.5, 3.5474)$. The first and second linear interpolations were done for the x coordinate, then the third interpolation was done for the y coordinate. The first and second interpolations are

$$p_{i1} = 3.6288 + (0.25 - 0) \frac{(3.5442 - 3.6288)}{(0.5 - 0)}$$

$$p_{i1} = 3.5865$$

and

$$p_{i2} = 3.6288 + (0.25 - 0) \frac{(3.5474 - 3.6288)}{(0.5 - 0)}$$

$$p_{i2} = 3.5069$$

where the subscripts $i1$ and $i2$ correspond to the first and second linear interpolation in the \mathbf{x} -coordinate, respectively.

The p_{i1} , p_{i2} , \mathbf{y}_1 and \mathbf{y}_3 were plugged in equation (23) again, then the third interpolation was done for the y coordinate to obtain the desired value p_{i3}

$$p_{i3} = 3.5865 + (0.25 - 0) \frac{(3.5069 - 3.5865)}{(0.5 - 0)}$$

$$p_{i3} = 3.5467$$

The model was generated meshed by using tetrahedral element, as shown in figure 23. The number of elements used on a 3D model is about 1,500,000 elements. The Elmer mesh file was provided a set of solvers, where was associated with the

electrostatic equation. In the equation section and solver-specific option, the steps were the same as in 2D model.

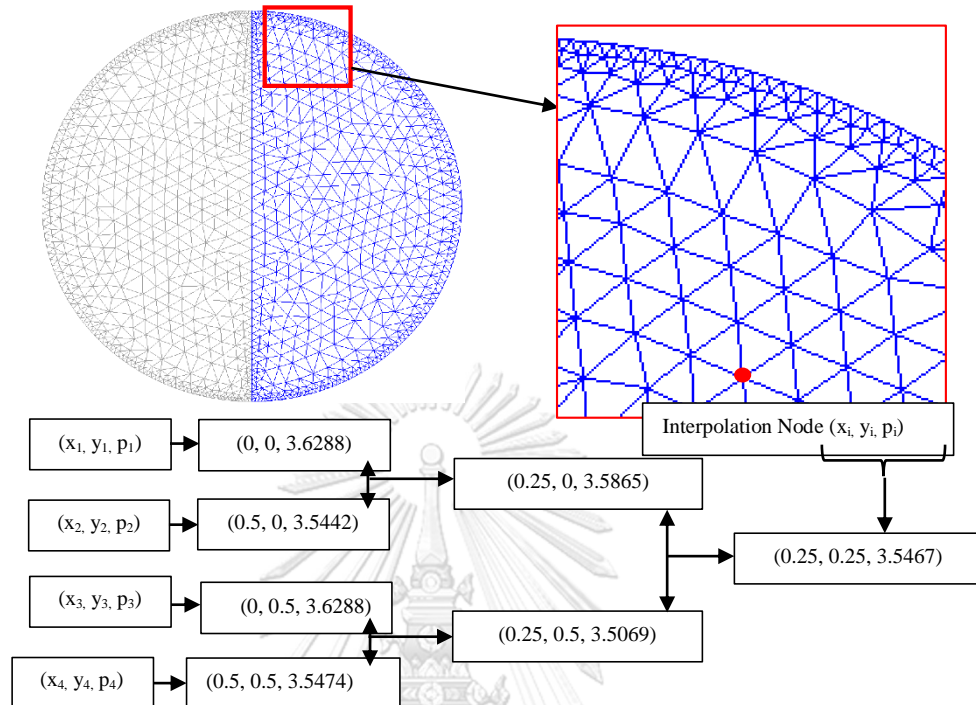


Figure 22 Bilinear interpolation method in 3D model

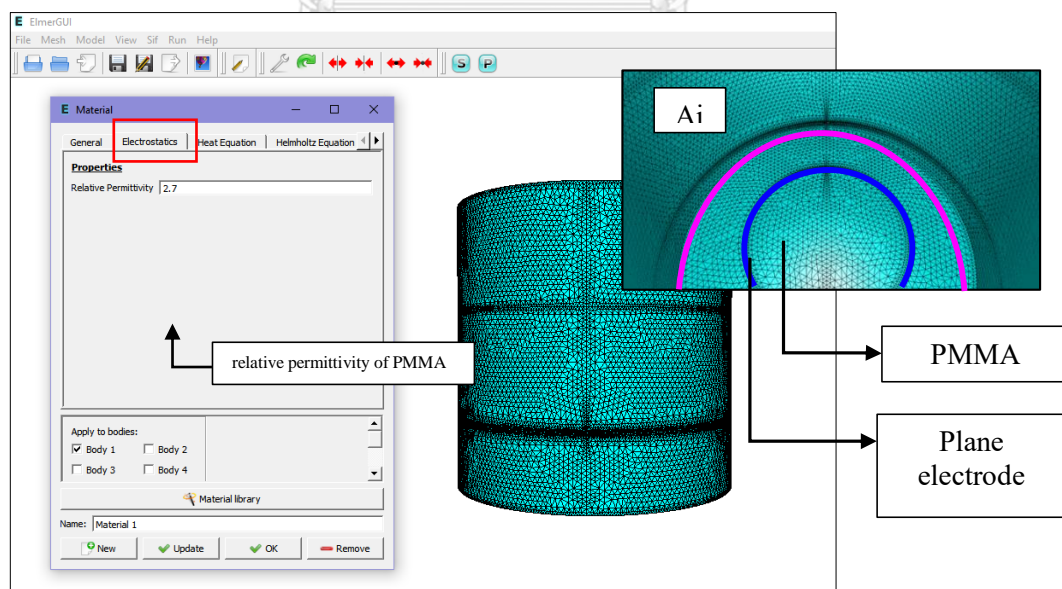


Figure 23 Equation setting of meshed 3-dimensional model in Elmer program

CHAPTER 5

RESULTS AND DISCUSSION

This chapter presents the experiment and simulation results of the 2D axisymmetric and 3D configurations described in Chapter 4. In the experiment, the potential on PMMA surface was measured between 0 and 24 hours. (approximately 90 minutes was taken for each measurement) The simulation results are shown as 3D surface potential on the $y=0$ line. The simulation results of electric field and surface charge density by the FEM are presented.

5.1 Experiment results

The surface potential is shown as 3D plots in figures 24-26. The vertical axis is the surface potential V_{sc} , and the horizontal axes are the position on the disc. It is seen that the surface potential of the 10-mm thick PMMA disc in figure 26 is lower than the other cases.

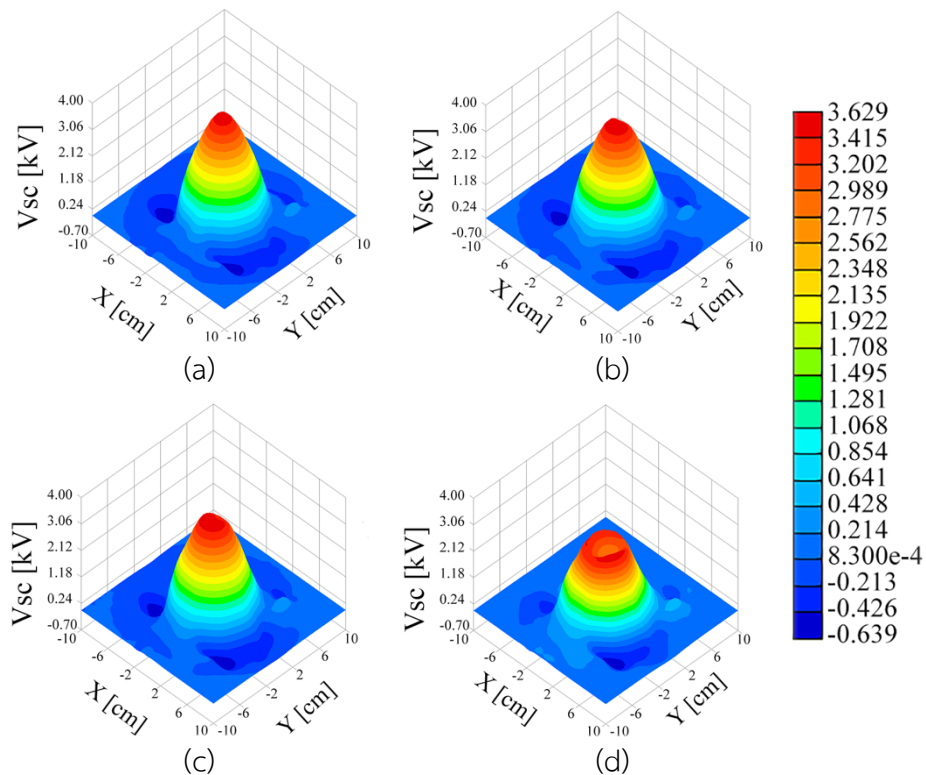


Figure 24 Surface potential on 1-mm thick PMMA disc at (a) 0 [h], (b) 3 [h], (c) 6 [h], and (d) 24 [h] after discharge application

Figure 24 shows the surface potential decay of a 1-mm thick PMMA disc from 0 to 24 hours after applying voltage. The potential distribution was initially symmetrically bell-shaped. The 3D plots show that the potential was slightly decreased at the center position then into a crater-like shape at 24 hours. The outer slope of distribution remained unchanged.

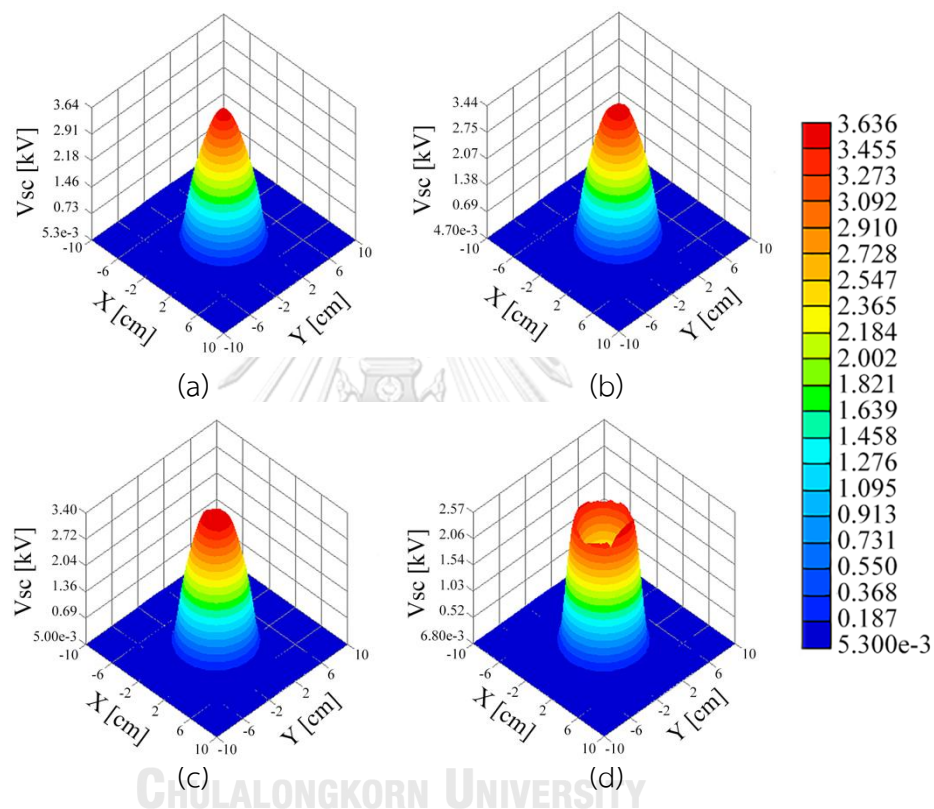


Figure 25 Surface potential on 2-mm thick PMMA disc at (a) 0 [h], (b) 3 [h], (c) 6 [h], and (d) 24 [h] after discharge application

Figure 25 shows the surface potential decay of a 2-mm thick PMMA disc from 0 to 24 [h] after discharge. The 3D distribution was initially symmetrically bell-shaped, as same as the 1-mm thickness. The surface potential decayed gradually with time. At 24 [h], the potential decreased remarkably at the center position until resembling a crater shaped. It can be seen that the peak was widened at 24 [h], and the outer slope was slightly increased.

In the case of 10-mm thick PMMA disc the surface potential decay is shown in figure 26. The potential distribution was initially asymmetrically bell-shaped then dropped rapidly from 3 [h] onwards, and mostly vanished at 24 [h]. It can be noticed that the surface potential of thin PMMA disc decayed slower than 10-mm thick PMMA disc.

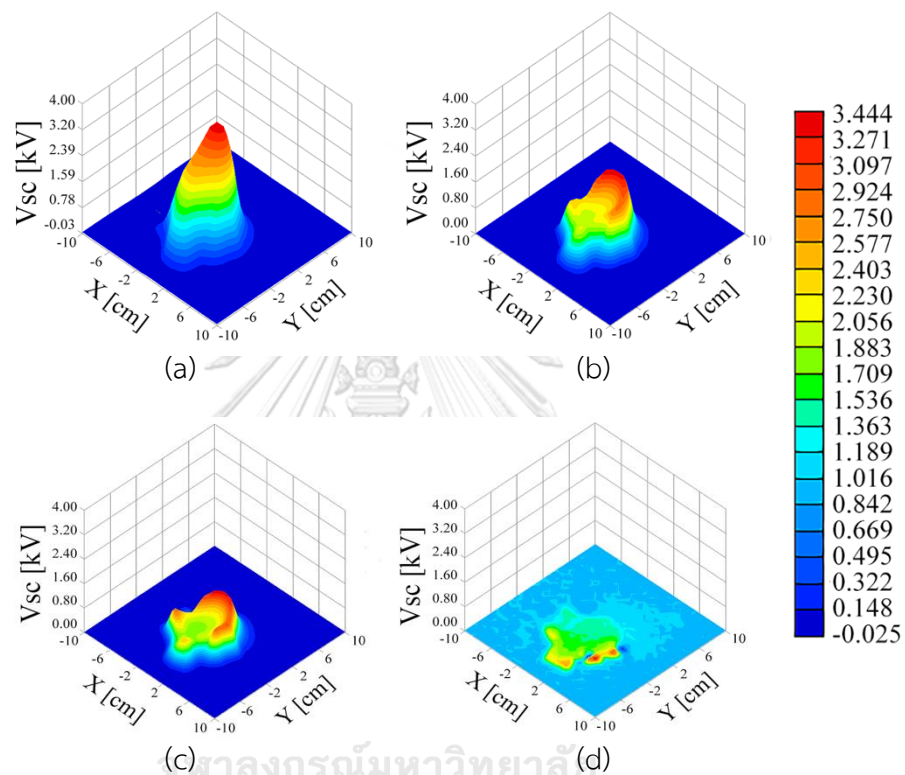


Figure 26 Surface potential on 10-mm thick PMMA disc at (a) 0 [h], (b) 3 [h], (c) 6 [h], and (d) 24 [h] after discharge application

The measurement results on the $y=0$ line is shown in figure 27. The surface potential of 1- and 2-mm thick PMMA disc slightly decreased between 0 and 6 hours and then obviously take a crater shape at 24 hours. In the case of 2-mm thickness, the surface potential spread in the same direction as the PMMA disc, and the outer slope of graph was slightly changed at 6 hours. On the 10-mm thickness disc, the potential decreased remarkably at the center position from 3 hours onward. Moreover, the figure 27(c) shows that the potential distribution was sunk overall. The potential distribution of 10-mm thick PMMA was narrow and decayed faster than that in the other cases.

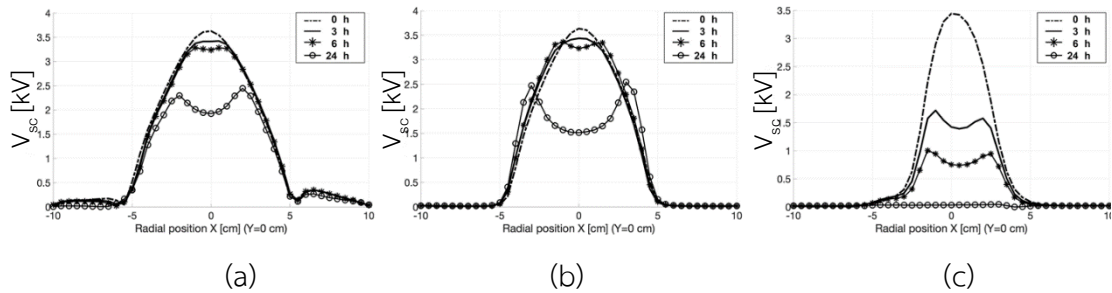


Figure 27 Surface potential decay with time on (a) 1-mm, (b) 2-mm, and (c) 10-mm thickness

From the measured potential, it can be estimated the surface charge density σ_{est} as

$$\sigma_{est} = \frac{\epsilon_0 \epsilon_r \phi_s}{t} \quad (19)$$

where ϕ_s is the measured surface potential. σ_{est} values from equation (19) are shown in figure 28. for 1-, 2- and 10-mm thickness discs at 0 hour after applying voltage. In case of 2- and 10-mm thick PMMA discs, the charge density were almost zero at 0.05 of radial position, and then remained stable to the edge of PMMA disc.

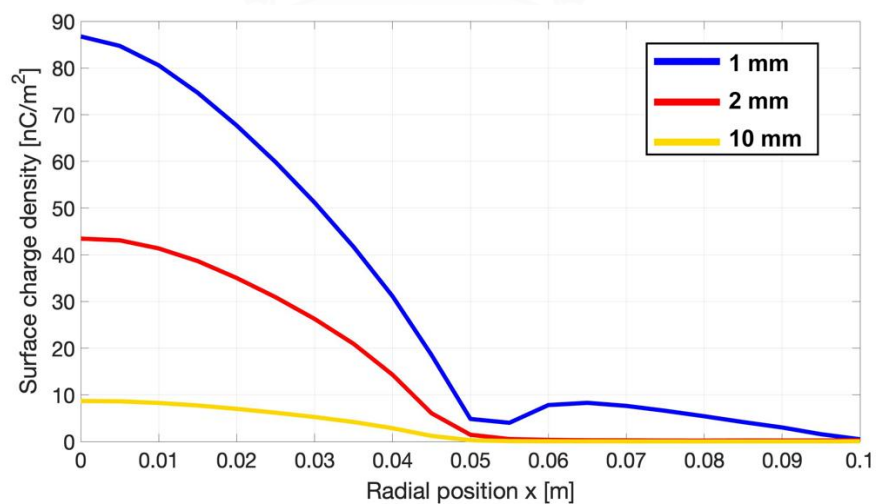


Figure 28 Estimated surface charge density on 1-, 2- and 10-mm thick PMMA at 0 [h]

5.2 Simulation results

5.2.1 2D simulation

The calculated potential resulting in 2D axisymmetric model is shown in figure 29. It can be seen that the potential distribution in the case of 10-mm thick PMMA disc was less than the thin cases. The field component on z-direction was obtained from the surface potential and the field component along the ρ direction may not be negligible.

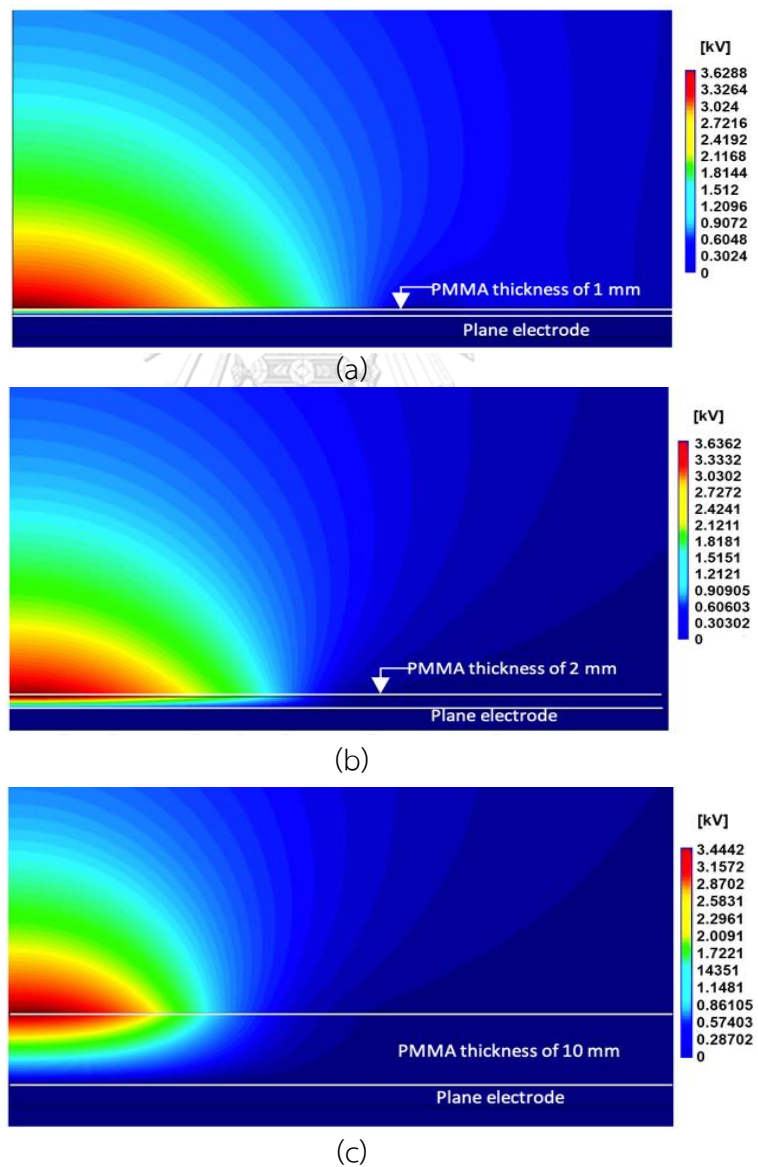


Figure 29 Calculated potential on (a) 1-, (b) 2-, and (c) 10-mm thick PMMA disc at 0[h]

The electric field in the airside and the upper surface of PMMA disc are shown in figure 30. The surface potential implied that electric field was more nonuniform in the 10-mm thick PMMA disc. It can be noted that electric field in PMMA disc was dependent on the thickness. In the airside, the field distribution of all cases were small. At the radial position of $\rho \approx 0.05$ m to the edge of PMMA sheet, the electric field on 2-, and 10-mm thickness were approximately equal zero. The electric field in the airside and the upper surface PMMA disc were used to calculate the surface charge density. The surface charge density on $y=0$ line is shown in figure 31. The surface charge density basically followed the similar tendency as the surface potential.

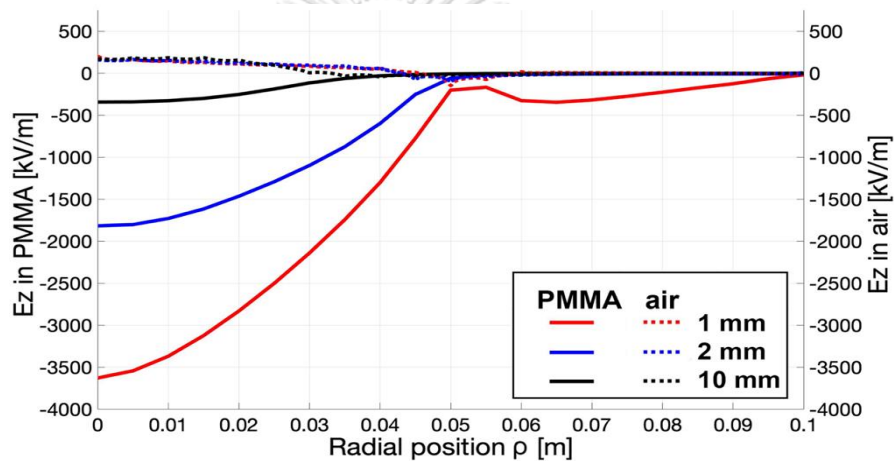


Figure 30 Electric field in the z-direction for 1-, 2- and 10-mm thick PMMA at 0 [h]

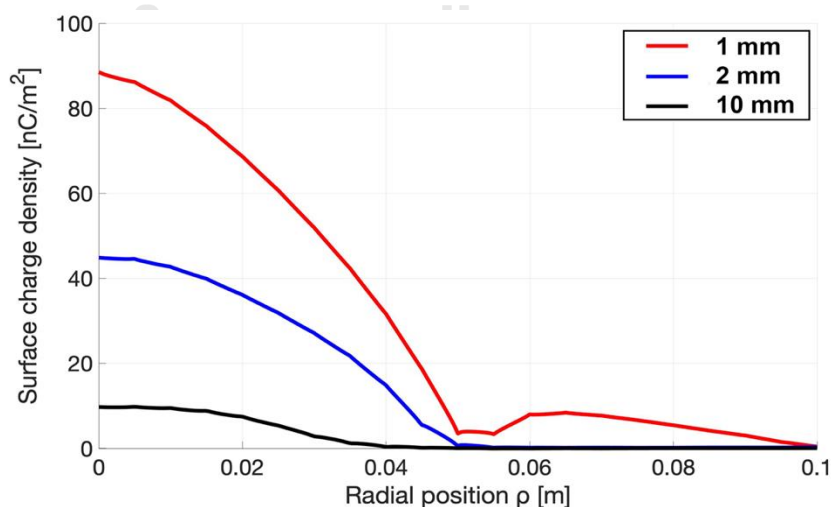


Figure 31 Surface charge density calculated by FEM of 1-, 2- and 10-mm thick PMMA at 0 [h]

5.2.2 3D simulation

The 3D calculation of potential resulting from GiD is shown in figure 32. In the cases of 1- and 2-mm thick PMMA disc, the calculated potential is wider than the 10-mm thickness. The electric field was calculated by FEM through the GiD and Elmer program.

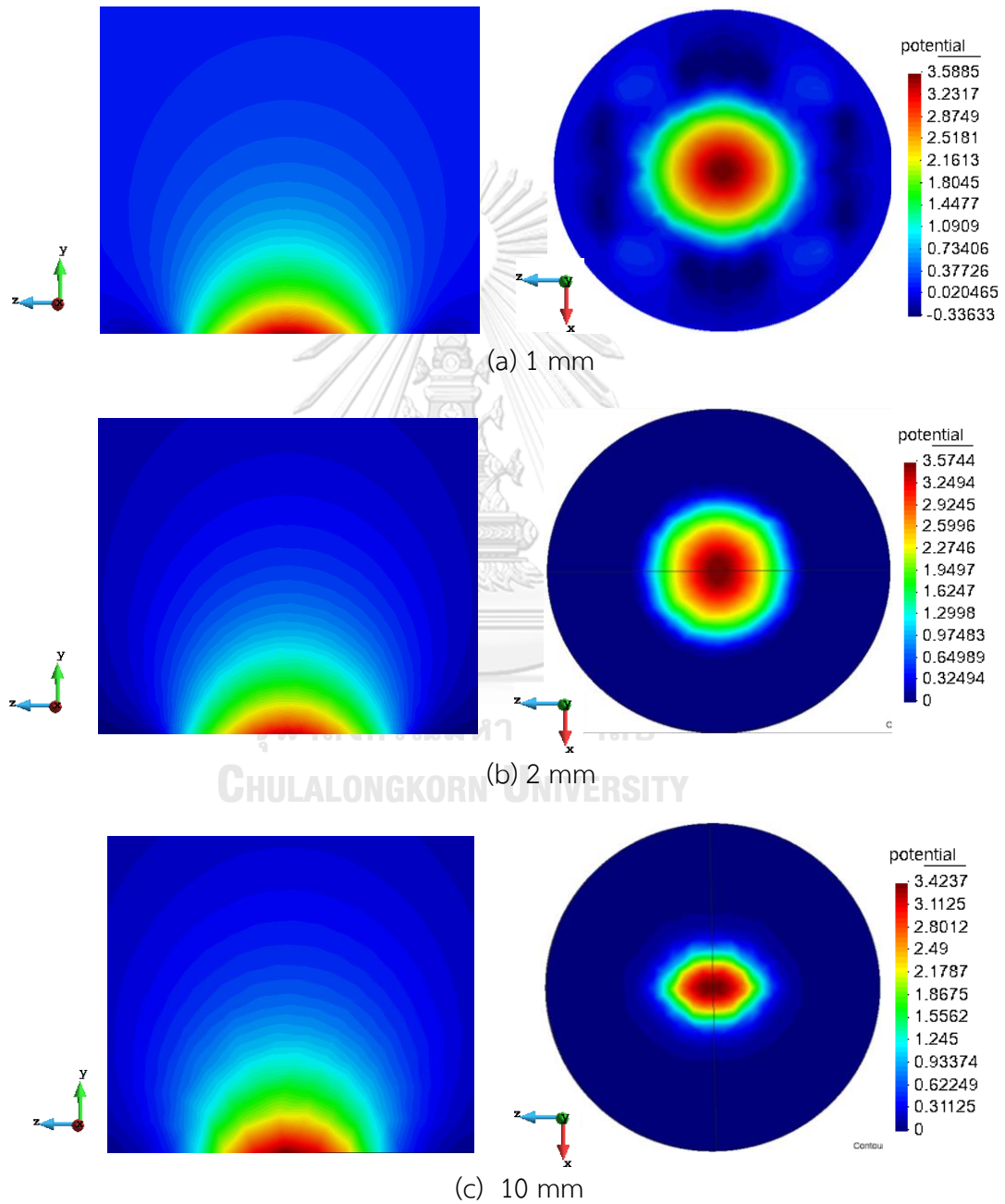


Figure 32 3D calculated potential of 1-, 2-, and 10-mm thick PMMA disc at 0 [h]

The 3D simulation results in the GiD program can be displayed or cut some parts of bodies by using switch volume sets on/off function. Figure 33 shows that the bodies of number 7 and 9 were cut off.

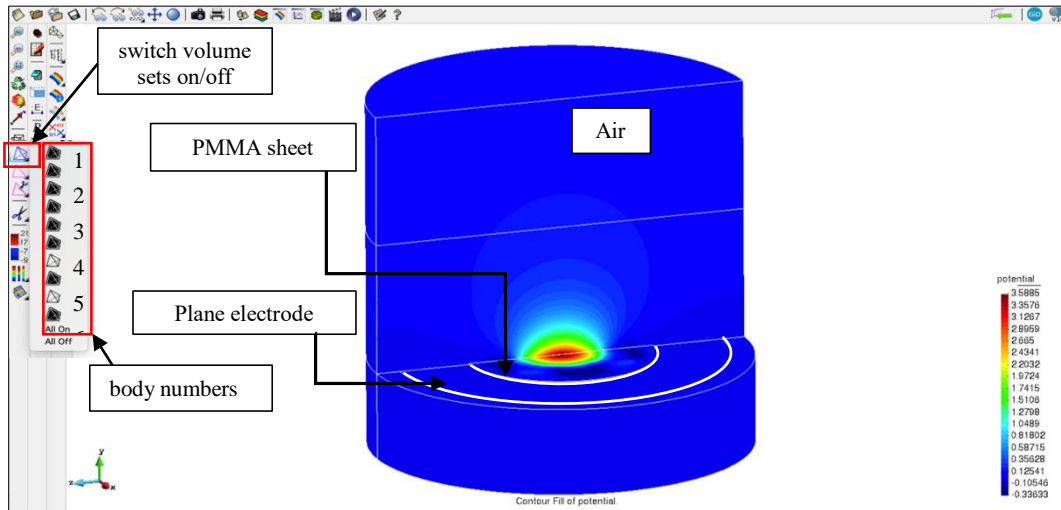
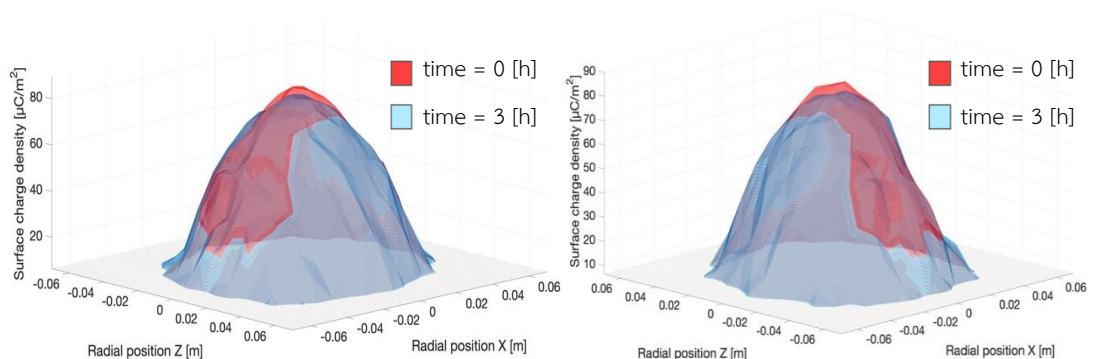


Figure 33 Simulation result of surface potential in GiD program

5.2.2.1 1-mm thickness PMMA disc

In this case, the surface charge density decayed gradually at the center position from 0 to 3 h, as illustrated in figure 34. The x- and z-axes range for display are only shown the plot from -0.07 to 0.07 m. Surface charge reduction clearly appeared at the peak which is shown in the red region. Lateral area of the distribution was increased, as shown in the blue area. The charge spread in the radial direction of the PMMA disc due to the mechanism of surface conduction [1-3].

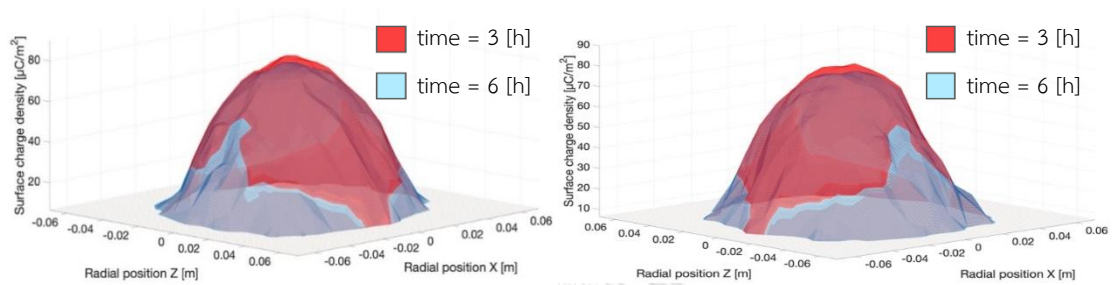


(a) 3D graph display from 0 to 180°

(b) 3D graph display from 180 to 360°

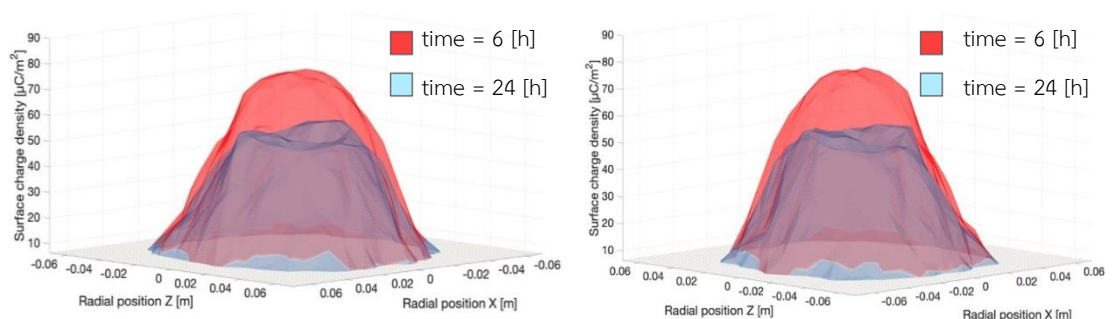
Figure 34 Calculated charge density on a 1-mm thick PMMA disc at 0-3 hours

Figure 35 compares the surface charge at 3 and that at 6 h. The charge density decreased overall as clearly seen in the red region. At the peak, the surface charge density was characterized by the development of a crater shape as shown in figure 35(a). The volume conduction and charge neutralization mechanisms [1-3] were related to the reduction of charge density. The blue area shows the increase of charge density which spread in the radial position, as shown in figure 35(b). The change in total charge for all calculation cases are shown in table 1.



(a) 3D graph display from 0 to 180° (b) 3D graph display from 180 to 360°
Figure 35 Calculated charge density on a 1-mm thick PMMA disc at 3-6 hours

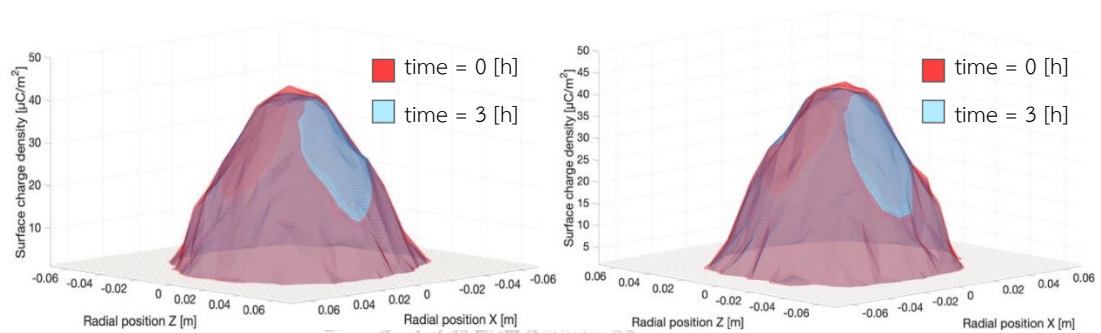
Figure 36 shows the surface charge at 6 and at 24 h. At 24 hours the charge density greatly decreased at the center position like a crater shape. This indicates that the charge neutralization mechanism affected directly to the reduction of charge density. Furthermore, the surface charge distribution was sunk overall, and the outer slope was moderately changed. The volume mechanism led to a characteristic of surface charge density during decay.



(a) 3D graph display from 0 to 180° (b) 3D graph display from 180 to 360°
Figure 36 Calculated charge density on a 1-mm thick PMMA disc at 6-24 hours

5.2.2.2 2-mm thickness PMMA disc

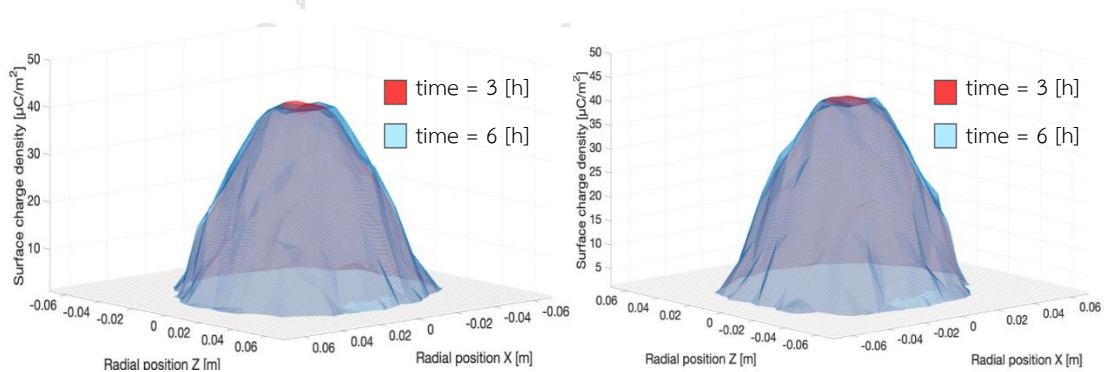
In this case, the surface charge at 0 h and 3 h is shown in figure 37. The x- and z-axes range for display are only shown the plot from -0.07 to 0.07 m. The decrease of charge density is seen as the red area. The peak was slightly decreased due to the charge neutralization mechanism [1-3]. At the blue area, the charge density increased possibly due to the surface conduction mechanism [1-3].



(a) 3D graph display from 0 to 180° (b) 3D graph display from 180 to 360°

Figure 37 Calculated charge density on a 2-mm thick PMMA disc at 0-3 hours

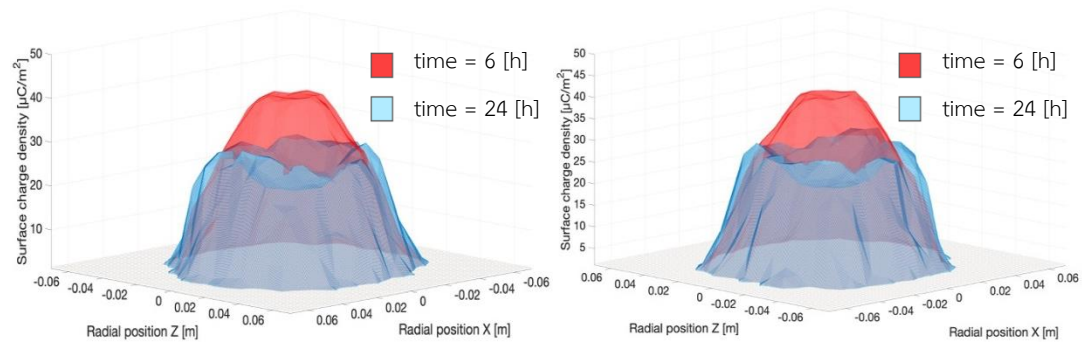
Figure 38 shows the surface charge density at 3 h and at 6 h. The charge density distribution was particularly decreased at the peak. Meanwhile, the area increased of charge density is expressed as the blue region. It can be explained by the mechanism of charge neutralization and surface conduction.



(a) 3D graph display from 0 to 180° (b) 3D graph display from 180 to 360°

Figure 38 Calculated charge density on a 2-mm thick PMMA disc at 3-6 hours

The surface charge decay at 6 h and at 24 h is shown in figure 39. The decrease of surface charge density to a crater shaped It is clearly seen. This result can be described by the field line depended on the charge neutralization mechanism. Figure 39 shows that the charge density increased and spread in the radial position due to the mechanism surface conduction [1-3].



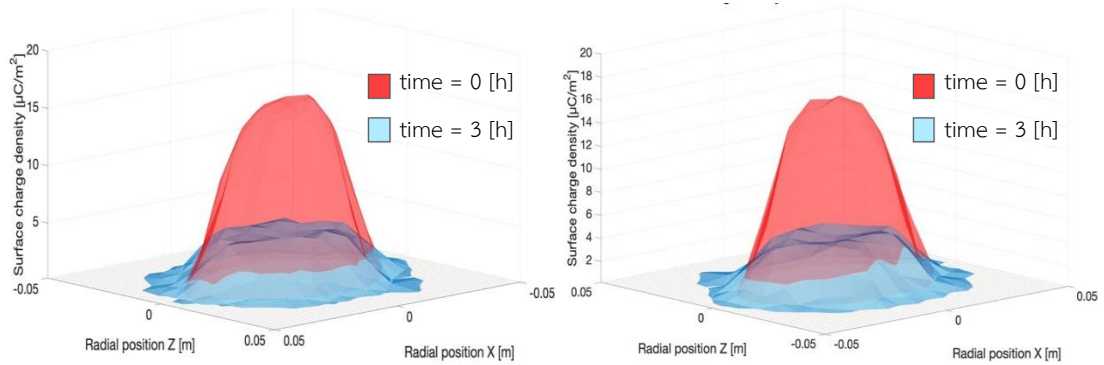
(a) 3D graph display from 0 to 180° (b) 3D graph display from 180 to 360°

Figure 39 Calculated charge density on a 2-mm thick PMMA disc at 6-24 hours

5.2.2.3 10-mm thickness PMMA disc

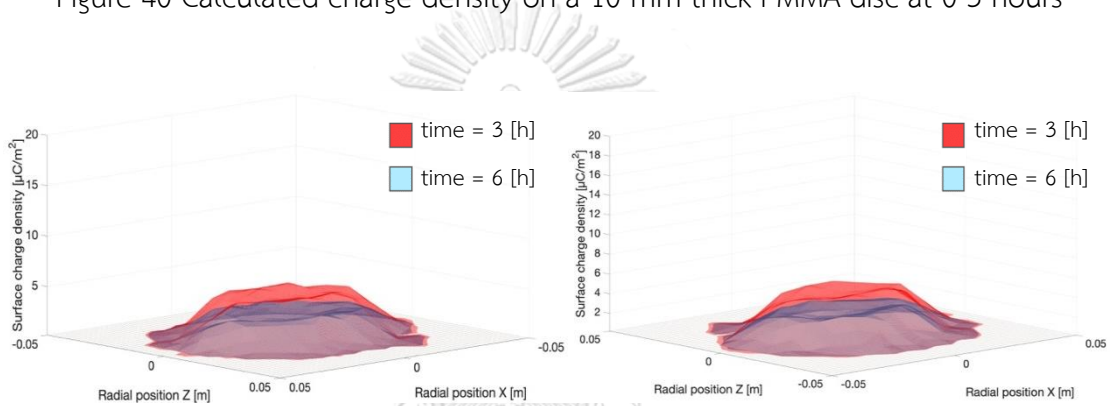
The surface charge at 0 h and 3 h is shown in figure 40. The x- and z-axes range for display are only shown the plot from -0.05 to 0.05 m. The surface charge decay was faster than the other cases. The mainly decrease appeared at the center position, which showed a crater shape. The blue area shows that the charge density increased and was slightly spread in the radial direction. The charge neutralization, surface and volume conduction mechanism contributed to the decrease of charge density.

Figure 41 shows the surface charge between 3 h and at 6 h. The surface charge density was mainly decreased at the center. The decay of space charge was due to the charge neutralization mechanisms [1-3]. Moreover, the charge density was decayed overall due to the volume mechanism. The charge density was almost equal zero at 24 h, as shown in figure 42.



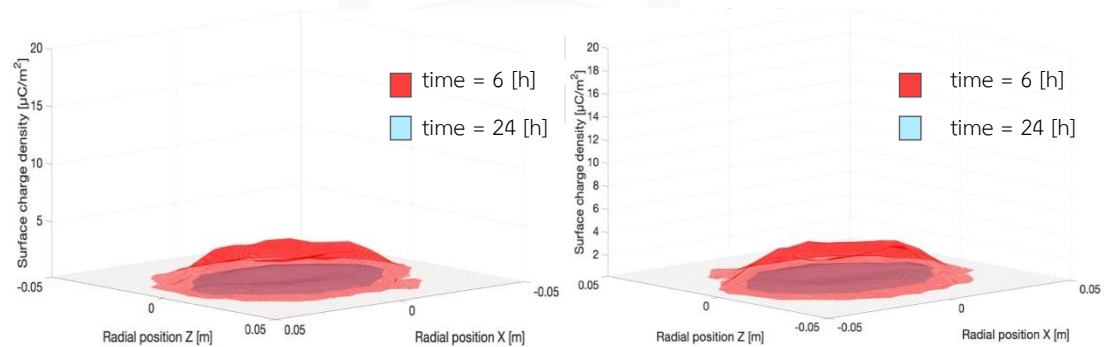
(a) 3D graph display from 0 to 180° (b) 3D graph display from 180 to 360°

Figure 40 Calculated charge density on a 10-mm thick PMMA disc at 0-3 hours



(a) 3D graph display from 0 to 180° (b) 3D graph display from 180 to 360°

Figure 41 Calculated charge density on a 10-mm thick PMMA disc at 3-6 hours



(a) 3D graph display from 0 to 180° (b) 3D graph display from 180 to 360°

Figure 42 Calculated charge density on a 10-mm thick PMMA disc at 6-24 hours

According to the 3D graph of surface charge density, the total charge in each cases were determined by using the integration. The limits of integration are on the x- and z-axes range for display. The total surface charge and change of charge with time

are shown in table 1 where “-” indicates a decrease of surface charge and “+” indicates an increase of surface charge.

Table 1 The total surface charge and different of charge on a 1, 2 and 10-mm thick PMMA disc

time	1-mm thickness PMMA disc		2-mm thickness PMMA disc		10-mm thickness PMMA disc	
	Total charge [μC]	Change of charge [μC]	Total charge [μC]	Change of charge [μC]	Total charge [μC]	Change of charge [μC]
0 [h]	0.3524	-	0.1565	-	0.0124	-
3 [h]	0.3577	+0.0053	0.1519	-0.0046	0.0106	-0.0018
6 [h]	0.3568	-0.0009	0.1599	+0.008	0.0072	-0.0034
24 [h]	0.2954	-0.0614	0.146	-0.0139	0.0012	-0.006

In the case of 1 and 2 mm thick PMMA sheets, the charge change at 0-3 hours and 3-6 hours were increased. The numerical results based on measurement might have error estimations. It can be explained that the accuracy of the calculation in these two cases might not be enough. In the case of 10-mm thickness, the surface charge was continually decreased with time.

As a result of measurement and numerical analysis, the surface charge density of all cases were formed as a crater like shape with time due to the mechanism of charge neutralization. The decrease rate of surface charge on a thicker disc was relatively fast in comparison to the thin PMMA discs. A surface charge on a PMMA disc will decay because of three main reasons consisted of the thickness of dielectric disc, varying with time, and the three mechanisms.

CHAPTER 6

CONCLUSIONS

Dielectric materials are essentially the insulators, which can be withstand the high electric field stress. Hence, it is important to understand physical phenomena related to surface charging. The thesis presents the experiments and simulations related to the behavior of surface charge decay. The surface charge decay on the PMMA disc was investigated to observe its behavior and dependency on the disc thickness.

6.1 Measurement results

In the case of 1- and 2-mm thick PMMA discs, the initial potential distributions were bell-shaped. In the case of the 10-mm thickness, the surface potential was asymmetrically bell-shaped and lower than the former two cases. The measured surface potential decreased with time and then characterized as a crater. For 24 hours, the surface potential of 1- and 2- mm thicknesses decreased mainly at center position. The surface potential on the (10-mm) thick PMMA disc almost equal zero. It can be described that the surface potential distribution of the thin PMMA disc decayed slower than the cases of thicker discs.

6.2 2D simulation results

The electric field on z-direction was obtained from the surface potential. The electric field in the PMMA disc depends on its thickness. In the air side, the electric field distributions of all cases were small. In the case of 2- and 10-mm thick PMMA disc, the electric field in the air side were approximately equal zero at the radial position of $\rho \approx 0.05$ m to the edge of PMMA sheet. The calculated surface charge density basically followed the similar tendency as the surface potential. The estimated surface charge density in the cases of 1- and 2-mm thick PMMA agreed well with the simulation one. In the case of 10-mm thickness, the estimated charge density was lower than the simulation one.

6.3 3D simulation results

A 3D calculation model illustrated the result much more clearly than a 2D simulation. Therefore, it can be seen that the surface potential distribution in the case of 1- and 2-mm thickness were symmetrical and larger than the thick (10-mm) PMMA disc. The field component on z-direction can be derived from the potential and then used to calculate the surface charge density.

The surface charge reduction process was investigated by considering thickness of PMMA disc, time and all three mechanisms. In the case of 1- and 2-mm thickness, these surface charge distributions were initially bell-shaped and was higher than the thicker disc. In the case of 10-mm thick PMMA disc, the initial surface potential distribution was narrow bell-shaped. It was observed that the decay of charge rapidly occurred during 3 h. The decay rate was faster than the two thin cases. After a time of 24 h, the charge in case of 1-mm thickness was evidently sunk overall due to the mechanism of volume conduction. In the case of 2-mm thick PMMA disc, the charge spread laterally along the surface of PMMA disc due to the surface conduction mechanism. In the case of 10-mm thick PMMA disc, the result of the decay showed almost equal zero.

It can be concluded that there are 3 mechanisms for surface charge to decrease and dissipate. The decay of charge is due to the three mechanisms included of electric conduction through the volume of the insulator, electric conduction along the surface of the insulator, and charge neutralization by gas ions. The charge distribution was the combination of electric conduction current mechanism explained by air-side electric field, and gas conduction mechanism.

This thesis has outlined the charge decay process on dielectric discs made of PMMA. Therefore, the study with another condition aims to better understand the behavior and charge decay mechanism. Future studies with different kinds of dielectric material, negative discharge, and in the case of a stack of dielectric discs might be considered.

REFERENCES

1. Kindersberger, J. and C. Lederle, Surface charge decay on insulators in air and sulfurhexafluorid - part I: simulation. IEEE Transactions on Dielectrics and Electrical Insulation, 2008. **15**(4): p. 941-948.
2. Kindersberger, J. and C. Lederle, Surface charge decay on insulators in air and sulfurhexafluorid - part II: measurements. IEEE Transactions on Dielectrics and Electrical Insulation, 2008. **15**(4): p. 949-957.
3. Matsumoto, T., et al., Experimental Investigation and Numerical Analysis of Surface Charge Decay on Acrylic and Glass Epoxy Multilayer Materials in Air. IEEE Transactions on Power and Energy, 2014. **134**(3): p. 203-209.
4. Du, Q., et al., Surface charge distribution on DC basin-type insulator. IEEE Transactions on Dielectrics and Electrical Insulation, 2019. **26**(1): p. 17-25.
5. Zhou, H., et al., Surface charge accumulation on 500kV cone-type GIS spacer under residual DC voltage. IEEE Transactions on Dielectrics and Electrical Insulation, 2018. **25**(4): p. 1230-1237.
6. Li, C., et al., Understanding surface charge accumulation and surface flashover on spacers in compressed gas insulation. IEEE Transactions on Dielectrics and Electrical Insulation, 2018. **25**(4): p. 1152-1166.
7. Cooke, C.M. Charging of insulator surfaces by ionization and transport in gases. in Conference on Electrical Insulation & Dielectric Phenomena - Annual Report 1981. 1981.
8. Nakanishi, K., et al., Surface Charging On Epoxy Spacer At Dc Stress In Compressed SF6 GAS. IEEE Transactions on Power Apparatus and Systems, 1983. **PAS-102**(12): p. 3919-3927.
9. Z. Qiu, J.R., S. Shu,, Air Insulation Prediction Theory and Applications. 2019.
10. William H. Hayt, J., John A. Buck Engineering Electromagnetics. 2019
11. Dechaumphai, P., Finite Element Method in Engineering. 2560.
12. O.C. Zienkiewicz, R.L.T.a.J.Z.Z., The Finite Element Method: Its Basis and Fundamentals. 2005.

13. Phongthanapanich, S., Finite Element Methods and Mesh Triangulation. 2560.
14. T. Miyazaiki, R.S., Y. Izawa, K. Nishijima, PET Film Surface Charge Decay Process due to Polarity Effect. Conference on Electrical and Information Technology Kyushu Branch Union, 2017: p. 519-520

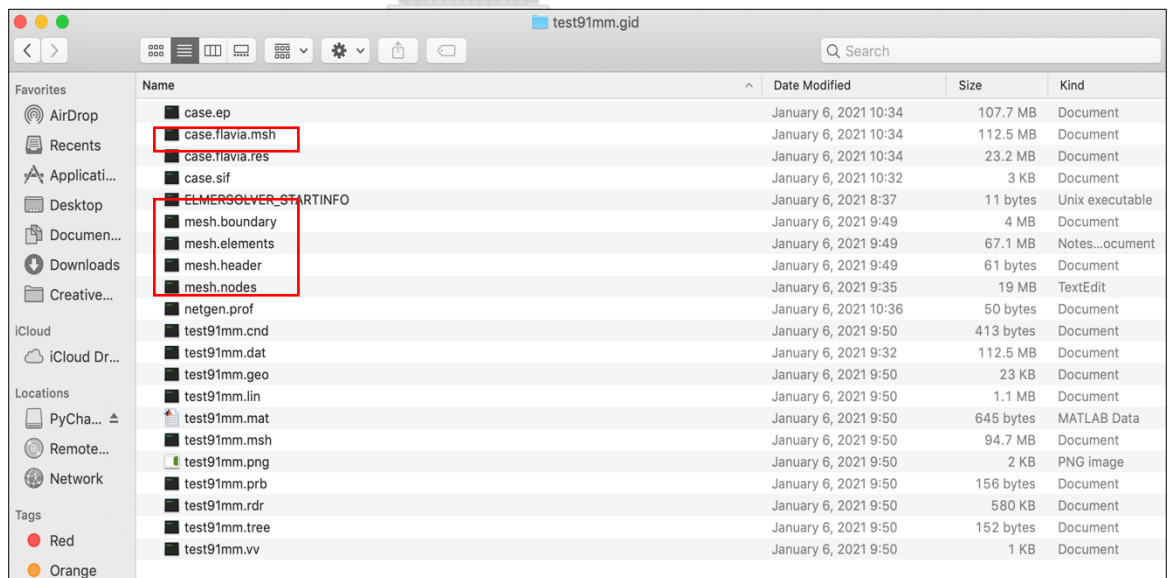


Appendix A

The procedure for importing the data set from Elmer program to MATLAB[®]

The information of mesh and calculated potential were generated from the Elmer program as a mesh file. The data files were imported to MATLAB[®] program for calculating the electric field and surface charge density. The procedure for importing the data set from Elmer program to MATLAB[®] follows

Step 1 The use of ElmerGUI software calculated finite element in the simulation model was exporting the data of the potential and the coordinates. The output formats of nodes, boundaries and materials are divided into four different files with suffixes of mesh files consisted mesh.boundary, mesh.elements, mesh.header, and mesh.nodes. The solver program can also give the data set of calculated potential and the coordinates with the extensions .flavia.res, which called case.flavia.res., as shown in figure 43.



Name	Date Modified	Size	Kind
case.ep	January 6, 2021 10:34	107.7 MB	Document
case.flavia.msh	January 6, 2021 10:34	112.5 MB	Document
case.flavia.res	January 6, 2021 10:34	23.2 MB	Document
case.sif	January 6, 2021 10:32	3 KB	Document
ELMERSOLVER_STARTINFO	January 6, 2021 8:37	11 bytes	Unix executable
mesh.boundary	January 6, 2021 9:49	4 MB	Document
mesh.elements	January 6, 2021 9:49	67.1 MB	Notes...ocument
mesh.header	January 6, 2021 9:49	61 bytes	Document
mesh.nodes	January 6, 2021 9:35	19 MB	TextEdit
netgen.prof	January 6, 2021 10:36	50 bytes	Document
test91mm.cnd	January 6, 2021 9:50	413 bytes	Document
test91mm.dat	January 6, 2021 9:32	112.5 MB	Document
test91mm.geo	January 6, 2021 9:50	23 KB	Document
test91mm.lin	January 6, 2021 9:50	1.1 MB	Document
test91mm.mat	January 6, 2021 9:50	645 bytes	MATLAB Data
test91mm.msh	January 6, 2021 9:50	94.7 MB	Document
test91mm.png	January 6, 2021 9:50	2 KB	PNG image
test91mm.prb	January 6, 2021 9:50	156 bytes	Document
test91mm.rdr	January 6, 2021 9:50	580 KB	Document
test91mm.tree	January 6, 2021 9:50	152 bytes	Document
test91mm.vv	January 6, 2021 9:50	1 KB	Document

Figure 43 Data files in case of 1-mm thick PMMA disc calculated from ElmerGUI

Step 2 The mesh files and case.flavia.msh. are generally created with notepad or text (TXT) file. The text (TXT) files were converted into Excel spreadsheets by open the Excel spreadsheet and click the “Data” tab. In the Get External Data group, click “From Text” and select the TXT file.

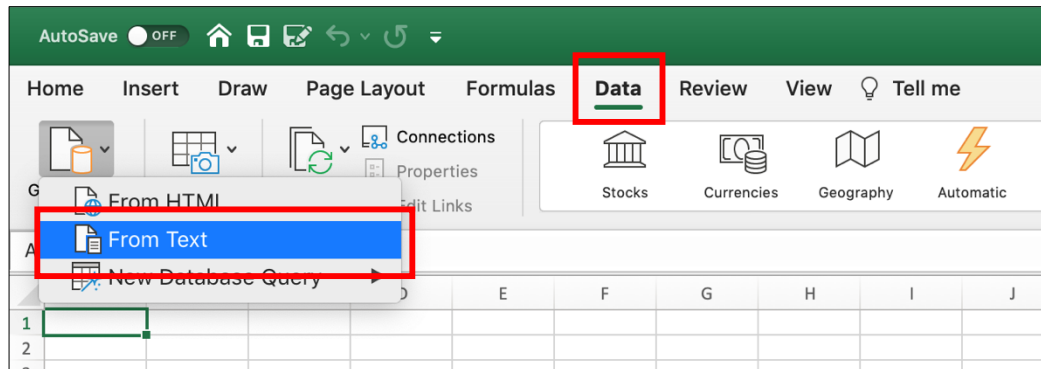


Figure 44 Display Data tap for selecting the TXT file

Step 3 Select "Delimited", "Tab" and "Space" when converting a TXT file.

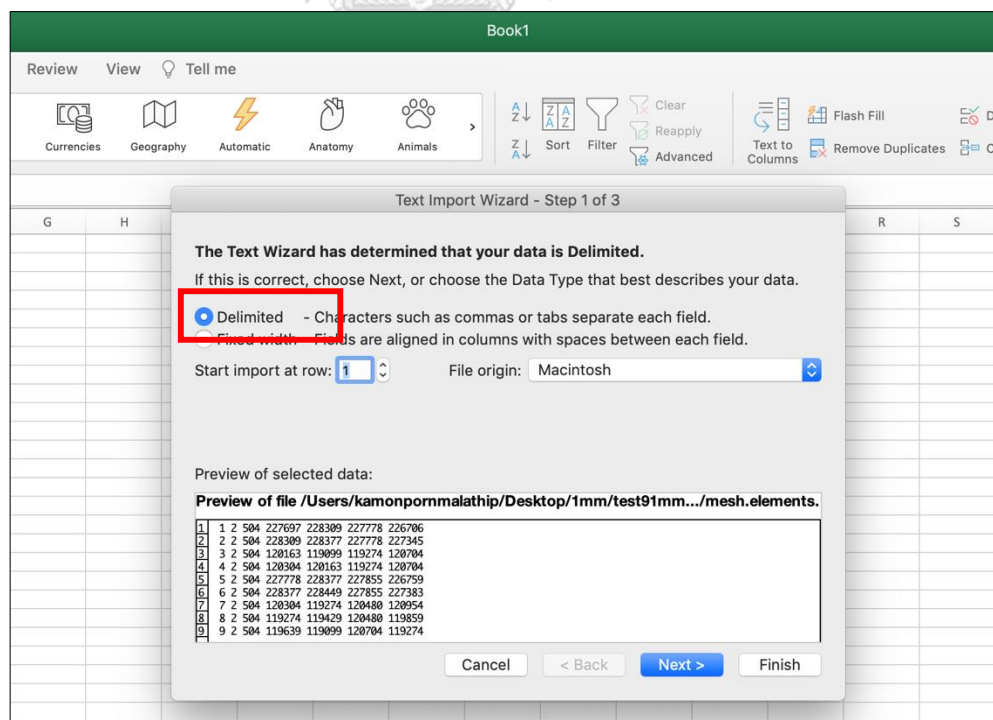


Figure 45 Display Text Import Wizard for selecting “Delimited”

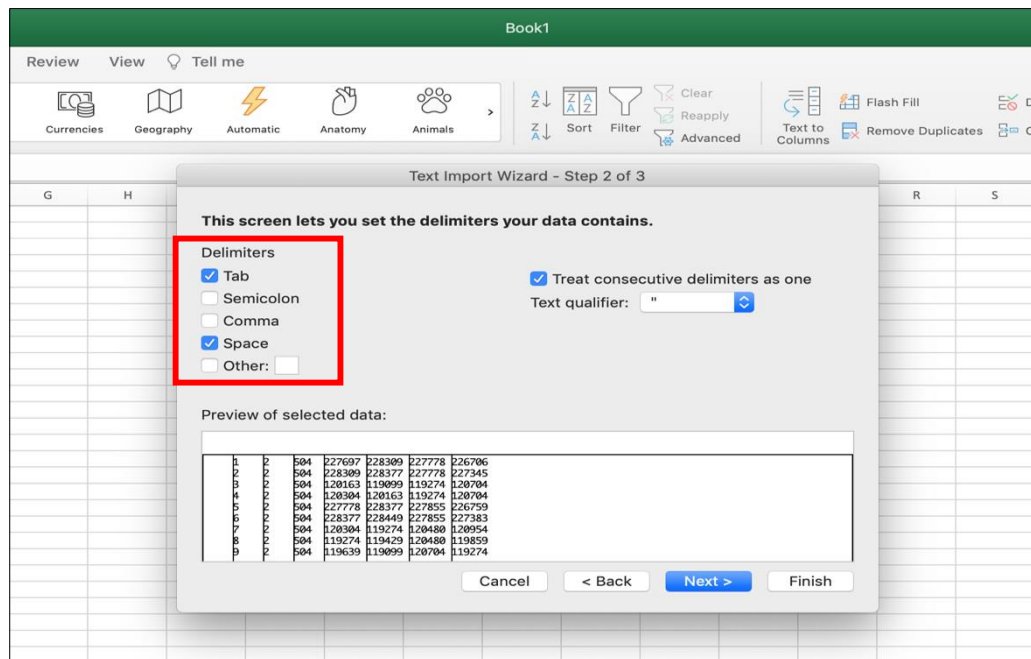


Figure 46 Display Text Import Wizard for selecting “Tab” and “Space”

Step 4 The information is sorted in the same pattern as in the TXT file. In order to import a spreadsheet into MATLAB program, the spreadsheet must be saved as a .xls file.

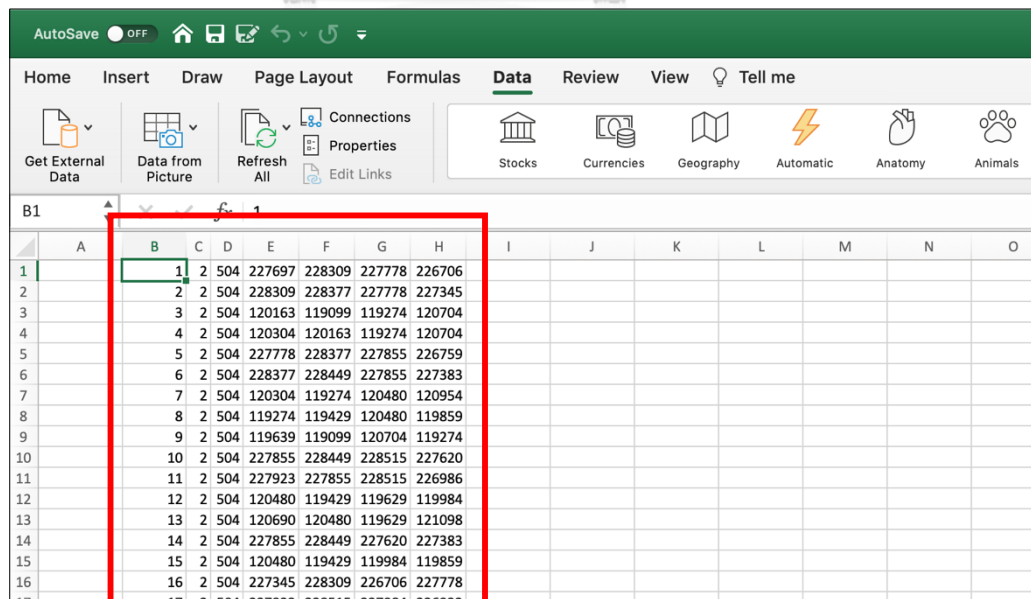


Figure 47 Display a spreadsheet of nodes data

Step 4 After save the data file, with file extension ".xls", launch MATLAB program and select "Import Data" from the file menu. Select "Numeric Matrix" data type, and then click the "Import Selection" button to import the data into the MATLAB workspace.

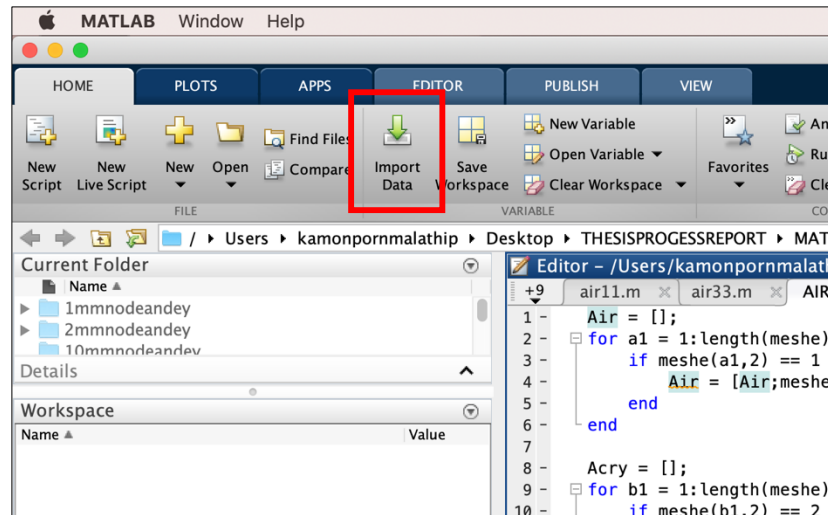


Figure 48 Display Import Data a tap for selecting the xls file

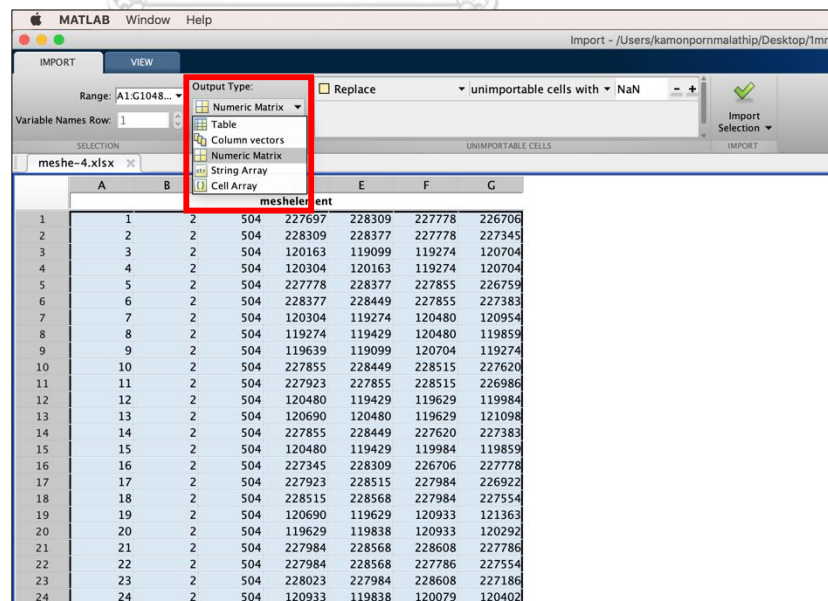


Figure 49 Display Import section for selecting the output type of "Numeric Matrix"

Appendix B

Elmer mesh files

mesh.header

```
nodes  elements  boundary-elements
types
type1  elements1
type2  elements2
...
typeN  elementsN
```

mesh.nodes

```
node1  tag1  x1  y1  z1
node2  tag2  x2  y2  z2
...
nodeN  tagN  xN  yN  zN
```

mesh.elements

```
element1  body1  type1  n11 ... n1M
element2  body2  type2  n21 ... n2M
...
elementN  bodyN  typeN  nN1 ... nNM
```

mesh.boundary

```
element1  boundary1  parent11  parent12  n11 ... n1M
element2  boundary2  parent21  parent22  n21 ... n2M
...
elementN  boundaryN  parentN1  parentN2  nN1 ... nNM
```



VITA

NAME Kamonporn Malathip

DATE OF BIRTH 05 December 1994

PLACE OF BIRTH โรงพยาบาลรวมแพทย์สุรินทร์

INSTITUTIONS ATTENDED มหาวิทยาลัยธรรมศาสตร์

HOME ADDRESS Nonsi Residence Bangkok, 619B, 87 ซอย นาวิ้น ถนน เชื้อเพลิง
ช่องนนทรี เขต ยานนาวา กรุงเทพฯ, สาทร, กรุงเทพฯ, ประเทศไทย,
10120

AWARD RECEIVED Best Paper Award at International Conference on
Condition Monitoring and Diagnosis 2020